

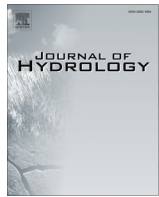


ELSEVIER

Contents lists available at ScienceDirect

Journal of Hydrology

journal homepage: www.elsevier.com/locate/jhydrol



Constructing river stage-discharge rating curves using remotely sensed river cross-sectional inundation areas and river bathymetry



Feifei Pan ^{a,*}, Cheng Wang ^b, Xiaohuan Xi ^b

^a Department of Geography and the Environment, University of North Texas, Denton, TX 76203, USA

^b Institute of Remote Sensing and Digital Earth, Chinese Academy of Sciences, Beijing 100094, China

ARTICLE INFO

Article history:

Received 4 February 2016

Received in revised form 1 June 2016

Accepted 11 June 2016

Available online 25 June 2016

This manuscript was handled by Konstantine P. Georgakakos, Editor-in-Chief, with the assistance of Jennifer Guohong Duan, Associate Editor

Keywords:

Landsat TM imagery

Digital elevation model

River bathymetry

The Manning's coefficient

The Manning's equation

Inundation area

River stage and discharge

The Bernoulli equation

Gradually varied open channel flow

Nonlinear constrained global optimization

ABSTRACT

Remote sensing from satellites and airborne platforms provides valuable data for monitoring and gauging river discharge. One effective approach first estimates river stage from satellite-measured inundation area based on the inundation area-river stage relationship (IARSR), and then the estimated river stage is used to compute river discharge based on the stage-discharge rating (SDR) curve. However, this approach is difficult to implement because of a lack of data for constructing the SDR curves. This study proposes a new method to construct the SDR curves using remotely sensed river cross-sectional inundation areas and river bathymetry. The proposed method was tested over a river reach between two USGS gauging stations, i.e., Kingston Mines (KM) and Copperas Creek (CC) along the Illinois River. First a polygon over each of two cross sections was defined. A complete IARSR curve was constructed inside each polygon using digital elevation model (DEM) and river bathymetric data. The constructed IARSR curves were then used to estimate 47 river water surface elevations at each cross section based on 47 river inundation areas estimated from Landsat TM images collected during 1994–2002. The estimated water surface elevations were substituted into an objective function formed by the Bernoulli equation of gradually varied open channel flow. A nonlinear global optimization scheme was applied to solve the Manning's coefficient through minimizing the objective function value. Finally the SDR curve was constructed at the KM site using the solved Manning's coefficient, channel cross sectional geometry and the Manning's equation, and employed to estimate river discharges. The root mean square error (RMSE) in the estimated river discharges against the USGS measured river discharges is $112.4 \text{ m}^3/\text{s}$. To consider the variation of the Manning's coefficient in the vertical direction, this study also suggested a power-law function to describe the vertical decline of the Manning's coefficient with the water level from the channel bed lowest elevation to the bank-full level. The constructed SDR curve with the vertical variation of the Manning's coefficient reduced the RMSE in the estimated river discharges to $83.9 \text{ m}^3/\text{s}$. These results indicate that the method developed and tested in this study is effective and robust, and has the potential for improving our ability of remote sensing of river discharge and providing data for water resources management, global water cycle study, and flood forecasting and prevention.

© 2016 Elsevier B.V. All rights reserved.

1. Introduction

River discharge, the volumetric rate of water flow passing a cross section of a river, is essential to water supply planning and management, reservoir management and operation, hydropower generation, flood prediction and control, understanding of the global water cycle, and other hydrological applications. Although we can directly measure river discharge through establishment and operation of river gauging stations, many watersheds in the world are ungauged or poorly-gauged for several reasons, such as the cost

to install and maintain gauging stations, inaccessible areas, and politically unstable regions, especially in developing countries. Even in some developed countries, the cost of installation and operation of gauging stations greatly limits the number of river gauging stations installed. For example, the cost for the United States Geological Survey (USGS) to install a gauging station is between \$20,000 and \$35,000, and the annual operational cost is about \$20,000 (e.g., Fekete and Vörösmarty, 2007). Because of a shortage of funding, the number of gauging stations in the United States is decreasing (e.g., Vorosmarty et al., 1996; IAHS, 2001; Bjerklie et al., 2003; Hannah et al., 2011). Many major flood events around the world were not adequately measured (Croke and Pappenberger, 2009), and many gauging network programs for

* Corresponding author.

E-mail address: feifei.pan@unt.edu (F. Pan).

worldwide major rivers, not to mention medium and small rivers, are shrinking (Hannah et al., 2011).

Directly measuring river discharge is often difficult because of the irregularity in river channels and variability of flow velocity in both vertical and horizontal directions. Therefore, to directly measure river discharge, a cross section is often divided into a number of sub-cross sections, and in each sub-cross section, a number of flow velocities at different flow depths are measured and averaged resulting a mean flow velocity for that sub-cross section. Then the river discharge is computed as the sum of all mean flow velocity multiplied by sub-cross section area. This method is also known as the velocity-area method (Mosley and McKerchar, 1992), but it is costly, labor intensive, and time consuming to directly measure river discharge using the velocity-area method. To save cost, labor and time, river discharge is usually inferred from the measurement of river stage based on the pre-defined or pre-observed stage-discharge rating (SDR) curve (Buchanan and Somers, 1969; Olson and Norris, 2005). River stage is the height of water surface above a nearby reference point. However, some field surveys to measure river discharge and stage simultaneously are still needed for constructing the SDR curve before the established gauging station at a cross section can be fully operational. Moreover, the stage-discharge relationship is not static but rather varies with time, since the processes of erosion and sediment deposition occurring in river channels and riverbanks can alter the shape of these channels. Therefore, a periodic check of SDR curves against the direct measurements is needed. This is yet another reason why maintaining river gauging stations is cost-, labor-, and time-intensive (Hannah et al., 2011).

In addition to the traditional stage-discharge rating curve method, the acoustic Doppler current profiler (ADCP) has evolved to be a useful tool for measuring streamflow since the 1990s (e.g., Morlock, 1996; Costa et al., 2000; Mueller, 2003; Simpson, 2001; Simpson and Oltmann, 1993; Mueller and Wagner, 2006; Oberg and Mueller, 2007; Mueller et al., 2013). The ADCP has three important advantages compared to the conventional current-meter discharge measurement: (1) the ADCP measurement is faster, (2) the ADCP can measure streamflow in highly dynamic and flood flows; and (3) the ADCP can measure continuous 3-D water velocity profiles (Hirsch and Costa, 2004). However, there are still some limitations associated with the ADCP, such as time required for post-processing data, the impact of the sediment concentrations on the accuracy of the ADCP velocity measurement, and un-measurable areas at the water surface and near the channel bed. In addition to these limitations, the ADCP's unfeasible nature of continuously monitoring discharge determines that the traditional rating curve method will still be the dominant method for continuously monitoring discharge at gauging stations around the world in the near future.

Since the 1990s, remote sensing of discharge and river stage has progressed rapidly (e.g., Smith, 1997; Alsdorf et al., 2007; Schumann et al., 2009; Pavelsky et al., 2014). Most remote sensing methods for measuring discharge and river stage published in the literature can be classified into four types: (1) estimating river stage and discharge using satellite-measured inundation area (e.g., Smith et al., 1995, 1996; Hamilton et al., 1996; Pietroniro et al., 1999; Al-Khudhairy et al., 2002; Xu et al., 2004; Zhang et al., 2004; Brakenridge et al., 2005, 2007; Temimi et al., 2005; Ashmore and Sauks, 2006; Smith and Pavelsky, 2008, 2009; Pan and Nichols, 2013; Pan, 2013; Pan et al., 2013; Cai et al., 2015); (2) measuring water surface elevation using satellite altimetry data (e.g., Koblinsky et al., 1993; Birkett et al., 2002; Coe and Birkett, 2004; Kouraev et al., 2004; Calmant and Seyler, 2006; Leon et al., 2006; Bhang et al., 2010; Jarihani et al., 2013); (3) integrating satellite observations with topographic data to determine river stage and discharge (e.g., Brakenridge et al., 1998; Bjerkle et al., 2005;

Matgen et al., 2007; Schumann et al., 2008a, 2008b; Tarpanelli et al., 2013; Gleason and Smith, 2014; Gleason et al., 2014; Pavelsky, 2014; Gleason and Wang, 2015); and (4) combining satellite data and hydraulic models to compute discharge (e.g., Bates et al., 1997, 2006; Horritt and Bates, 2002; Andreadis et al., 2007; Roux et al., 2008; Durand et al., 2008, 2014; Jung et al., 2013; Domeneghetti et al., 2014).

Among these four types of methods, the first approach to estimate discharge and river stage using the satellite-measured inundation area (SMIA) is more popular and commonly used. One possible reason for this popularity is that inundation area is relatively easy to measure from space compared with altimetry point measurements of water surface elevation. Another reason is that rapid advances in optical and microwave remote sensing technology have produced a large number amount of high-resolution satellite and airborne images (e.g., QuickBird, WorldView, and GeoEye). However, the SMIA is usually used to estimate river stage first, and then discharge is determined based on the stage-discharge rating (SDR) curve. To estimate river stage from the SMIA, it is necessary to use the inundation area – river stage relationship (IARSR). Smith (1997) showed that the relationship between inundation area and water level is unique and can be used to estimate river stage. However, observed data for constructing the IARSR are often insufficient. For ungauged watersheds, river stage measurements are not available. For gauged watersheds, river stage measurements may be available, but the river stage measurements may not have been recorded on the same days as the inundation areas were measured from space.

One possible approach to construct the IARSR is to use the SMIA along with satellite-measured river stage at the same cross section measured at the same time. The inundation area is generally estimated from optical or microwave satellite imagery, and water surface elevation can be determined from satellite-borne radar or lidar data. Since inundation area and water surface elevation measurements are obtained from different satellites at times that seldom coincide, these satellite measurements cannot be used to construct the IARSR. A future satellite launch may solve this problem. NASA's Surface Water Ocean Topography (SWOT) mission, capable of measuring both water elevation and inundation area at the same time and providing invaluable data for hydrologists (Biancamaria et al., 2015; Durand et al., 2014; Pavelsky et al., 2014; Garambois and Monnier, 2015), is in the planning stage. While the SWOT mission has great potential, the satellite will not be launched until 2020, so there are still uncertainties associated with the mission. Therefore, there are two challenging problems associated with remote sensing of river stage and discharge at ungauged river cross sections using the satellite-measured inundation area: (1) how can IARSR curves be constructed without ground-based river stage measurements? and (2) how can SDR curves be constructed without ground-based river discharge measurements?

River stage refers to water surface elevation relative to a reference level known as a datum. Unlike direct satellite altimetry water surface elevation measurements, optical or microwave satellites can only provide information on the boundary between water body and dry riverbanks or the flooded area, without any direct information about water surface elevation. To utilize satellite imagery to retrieve river stage, a relationship between river stage and the boundary between water body and riverbanks or inundation area must be established first. There are several studies on this issue that established relationship between river stage and channel width (Pavelsky, 2014), or matched ground control points along riverbanks (Xu et al., 2004; Zhang et al., 2004). Since a channel width at a particular river stage is determined only by two points which are the water edges on the right and left riverbanks, the channel width approach is similar to matching ground control

points. However, only two sampling points could cause a great uncertainty in the estimated river stage. Through increasing sampling points by tens to hundreds to improve accuracy of the estimated river stage, Pan and Nichols (2013) proposed a method to construct the IARSR curve in a pre-defined polygon from digital elevation model (DEM) data. However, the constructed IARSR curves in Pan and Nichols (2013) are only applicable at river stages above the water surface elevation inside the pre-defined polygon detected by the DEM data. This study will first demonstrate that a complete IARSR curve can be constructed starting from the channel bed using combined DEM and river bathymetry (or channel bed elevation), also known as digital terrain model (DTM) data, and the constructed IARSR curve can be used to estimate river stage from the satellite measured inundation area over a wide dynamic range of flow conditions.

The traditional method to construct the SDR curves, which has been widely used by gauging stations in the United States and almost every other country around the world, is to simultaneously measure river stage and discharge at the river cross section of interest. River stage is relatively easy to measure; while river discharge can be directly measured using the velocity-area method (Mosley and McKerchar, 1992). Although this method is effective and can yield accurate measurements, it is time-consuming and labor intensive, and it might be dangerous to carry out such measurement in deep and torrential flow. The acoustic Doppler current profiler (ADCP) has the potential for easily and safely measuring discharge. Some studies have demonstrated that the rating curves can also be constructed through single velocity measurements coupled with the entropy method (e.g., Chiu and Abidin Said, 1995; Moramarco and Singh, 2010; Alessandrini et al., 2013; Farina et al., 2014).

To improve our ability to measure river discharge, especially at ungauged river cross sections using satellite imagery, this study proposes an approach to construct the SDR curves using the remotely sensed river cross-sectional inundation areas and river bathymetry without any direct river discharge measurements. The essence of the proposed method is to solve the Manning's coefficient based on the energy balance equation (i.e., the Bernoulli equation) of gradually varied open channel flow along a river reach between two cross sections. Using the solved Manning's coefficient, channel cross sectional geometry and the Manning's equation, we can construct the SDR curves at the upstream and downstream cross sections. The arrangement of this paper is as follows. Section 2 describes the theoretical background and methods proposed in this study. Section 3 introduces the study area and data. Results and discussion are presented in Section 4. Section 5 is a summary.

2. Methodology

2.1. Theoretical background

The river stage-discharge rating (SDR) curve considers the discharge as a single function of the stage (Braca, 2008) and is commonly used to estimate river discharges from measured river stages. The most commonly used rating curve function is a power law function (e.g., Herschy, 1995; Kennedy, 1984; Rantz et al., 1982a, 1982b; Mosley and McKerchar, 1992; Sauer, 2002):

$$Q = c_1(h - c_2)^{c_3} \quad (1)$$

where Q is the discharge, h is the stage, c_1 , c_2 , and c_3 are calibration coefficients. The power-law rating curve function shown in Eq. (1) actually can be derived from the Manning's equation (e.g., Henderson, 1966; Sturm, 2001) given as follows (Sauer, 2002):

$$U = \frac{1}{n} R^{2/3} S_e^{1/2}, \quad Q = UA = \frac{1}{n} AR^{2/3} S_e^{1/2} \quad (2)$$

where U is the mean velocity in m/s, Q is the discharge in m^3/s , n is the Manning's coefficient in $\text{s}/\text{m}^{1/3}$, S_e is the energy line slope (dimensionless), R is the hydraulic radius and equals to the ratio of the channel cross-sectional area A to the wetted perimeter. The units of R and A are m and m^2 , respectively. Under the uniform flow condition, the energy line slope is equal to the channel bed slope. However, if the channel geometry at a cross section and the channel bed slope are known through field survey, it is still hard to apply the Manning's equation (i.e., Eq. (2)) to construct the SDR curve, because the Manning's coefficient n also depends on the channel roughness, which is almost impossible to measure directly (Hornberger et al., 2014; Sturm, 2001). Usually the Manning's coefficient n at a river cross section is calculated based on the Manning's equation and river discharge and stage measured simultaneously. To address the difficulty in the estimation of the Manning's coefficient, this study proposes a method to determine the Manning's coefficient using remotely sensed inundation areas at two cross sections along a river reach and then the estimated Manning's coefficient can be used to construct the SDR curves without any ground-based river discharge measurements.

The proposed method is based on the energy conservation equation (i.e., the Bernoulli equation) of gradually varied open channel flow (Sturm, 2001) along a river reach between two cross sections:

$$z_1 + \alpha_1 \frac{U_1^2}{2g} = z_2 + \alpha_2 \frac{U_2^2}{2g} + h_L \quad (3)$$

where z_1 and z_2 are the water surface elevations, U_1 and U_2 are the mean velocities, α_1 and α_2 are the kinetic energy correction factors, at upstream and downstream cross sections, respectively, and h_L is the head loss from upstream to downstream. If between the upstream and downstream cross sections there are no major tributaries flowing into the channel or the distance between the upstream and downstream is short, the lateral inflow in Eq. (3) generally can be neglected. There are two contributors to the head loss, i.e., friction and channel expansion or contraction (Sturm, 2001), which can be estimated as follows:

$$h_L = \bar{S}_e L + k_L \left| \alpha_1 \frac{U_1^2}{2g} - \alpha_2 \frac{U_2^2}{2g} \right| \quad (4)$$

where \bar{S}_e is the mean slope of the energy line, L is the reach length, and k_L is the minor head loss coefficient due to channel expansion or contraction (Sturm, 2001). Replacing h_L in Eq. (3) by Eq. (4), yields:

$$z_1 + \alpha_1 \frac{U_1^2}{2g} = z_2 + \alpha_2 \frac{U_2^2}{2g} + \bar{S}_e L + k_L \left| \alpha_1 \frac{U_1^2}{2g} - \alpha_2 \frac{U_2^2}{2g} \right| \quad (5)$$

According to the Manning's equation, the mean velocities at two cross sections are as follows:

$$U_1 = \frac{1}{n_1} R_1^{2/3} S_{e1}^{1/2}, \quad U_2 = \frac{1}{n_2} R_2^{2/3} S_{e2}^{1/2} \quad (6)$$

where n_1 and n_2 are the Manning's coefficients, R_1 and R_2 are the hydraulic radii, and S_{e1} and S_{e2} are the energy line slopes at the upstream and downstream cross sections, respectively. Substituting Eq. (6) into Eq. (5), yields:

$$\begin{aligned} z_1 + \alpha_1 \frac{R_1^{4/3} S_{e1}}{2gn_1^2} &= z_2 + \alpha_2 \frac{R_2^{4/3} S_{e2}}{2gn_2^2} + \bar{S}_e L \\ &\quad + k_L \left| \alpha_1 \frac{R_1^{4/3} S_{e1}}{2gn_1^2} - \alpha_2 \frac{R_2^{4/3} S_{e2}}{2gn_2^2} \right| \end{aligned} \quad (7)$$

In the above equation, the water surface elevations (i.e., z_1 and z_2) can be directly measured by satellite altimeters or through in-situ monitoring, or estimated from satellite measured inundation areas (SMIA). This study will focus on estimating water surface elevations using the SMIAAs. The hydraulic radii and the reach length can be estimated from DEM data and river bathymetry. Therefore, there are five unknowns in Eq. (7), which are α_1 , α_2 , n_1 , n_2 , and k_L . To solve these five unknowns, we first need to obtain m ($m > 5$) pairs of water surface elevation measurements at the upstream and downstream cross sections to form an objective function based on Eq. (7) as follows:

$$\Phi = \sum_{i=1}^m \left[z_{1i} + \alpha_1 \frac{R_{1i}^{4/3} S_{e1}}{2gn_1^2} - z_{2i} - \alpha_2 \frac{R_{2i}^{4/3} S_{e2}}{2gn_2^2} - \bar{S}_e L \right. \\ \left. - k_L \left| \alpha_1 \frac{R_{1i}^{4/3} S_{e1}}{2gn_1^2} - \alpha_2 \frac{R_{2i}^{4/3} S_{e2}}{2gn_2^2} \right|^2 \right] (8)$$

Then these five unknowns can be solved using the least squares method or some nonlinear constrained global optimization schemes to minimize the objective function Φ given in Eq. (8). In addition to these five unknowns, the energy line slopes in Eq. (8), which are difficult to directly measure, also need to be determined. To solve this problem, we assume that the energy line slope S_e is a function of the channel bed slope S_b as follows:

$$S_{e1} = b_1 S_{b1}, \quad S_{e2} = b_2 S_{b2}, \quad \bar{S}_e = (b_1 S_{b1} + b_2 S_{b2})/2 \quad (9)$$

where S_{b1} and S_{b2} are channel bed slopes at the upstream and downstream stations, and b_1 and b_2 are two parameters representing ratios between the energy line slope and channel bed slope at the upstream and downstream cross sections, respectively. In this study we assume that these two parameters (i.e., b_1 and b_2) are constant under the steady state flow condition and the constructed steady state rating curve can be considered as a first order approximation. Actually the steady state rating curve is very useful and widely used around the world for estimating river discharge from measured river stage, although it has errors and uncertainties, especially as flow in natural channels greatly departs from a steady state flow.

With introducing two extra parameters (i.e., b_1 and b_2), the objective function Φ becomes:

$$\Phi = \sum_{i=1}^m \left[z_{1i} + \alpha_1 \frac{R_{1i}^{4/3} b_1 S_{b1}}{2gn_1^2} - z_{2i} - \alpha_2 \frac{R_{2i}^{4/3} b_2 S_{b2}}{2gn_2^2} - \frac{(b_1 S_{b1} + b_2 S_{b2})}{2} L \right. \\ \left. - k_L \left| \alpha_1 \frac{R_{1i}^{4/3} b_1 S_{b1}}{2gn_1^2} - \alpha_2 \frac{R_{2i}^{4/3} b_2 S_{b2}}{2gn_2^2} \right|^2 \right] \quad (10)$$

Now there are seven unknowns in the objective function Φ , which greatly increase uncertainty in the solutions of Eq. (10). To reduce uncertainty, in this study we use the reach average hydraulic characteristics to represent the corresponding hydraulic properties at the upstream and downstream cross sections as follows:

$$\alpha_1 = \alpha_2 = \alpha, \quad n_1 = n_2 = n, \quad b_1 = b_2 = b, \quad S_{b1} = S_{b2} = S_b \quad (11)$$

where α , n , b , S_b are the reach average kinetic energy correction factor, Manning's coefficient, the ratio of energy line slope to channel bed slope, and channel bed slope, respectively. Therefore, Eq. (10) is reduced to:

$$\Phi = \sum_{i=1}^m \left[z_{1i} + \alpha \frac{R_{1i}^{4/3} b S_b}{2gn^2} - z_{2i} - \alpha \frac{R_{2i}^{4/3} b S_b}{2gn^2} - b S_b L \right. \\ \left. - k_L \left| \alpha \frac{R_{1i}^{4/3} b S_b}{2gn^2} - \alpha \frac{R_{2i}^{4/3} b S_b}{2gn^2} \right|^2 \right] \quad (12)$$

The four unknowns (i.e., α , n , b , and k_L) in Eq. (12) can be solved using some nonlinear constrained global optimization schemes. After solving the Manning's coefficient, the SDR curves at the upstream and downstream cross sections can be established using the Manning's equation.

2.2. Flowchart

To explain the proposed method, a flowchart is shown in Fig. 1, which provides an overview of seven steps to construct the SDR curves using remotely sensed river cross-sectional inundation areas and river bathymetry. These seven steps are: (1) define a polygon that covers the cross section where the SDR curve is to be constructed; (2) select a downstream cross section and define a polygon that covers this cross section; (3) construct the complete IARSR curves inside both polygons using DEM and river bathymetric data; (4) estimate river inundation areas in both polygons using satellite images; (5) compute river stages at both cross sections based on the estimated inundation areas and the constructed IARSR curves; (6) form the objective function Φ (i.e., Eq. (12)) using the estimated river stages, and solve the Manning's coefficient using the nonlinear constrained global optimization method; (7) construct the SDR curves using the Manning's equation and the solved Manning's coefficients at upstream and downstream cross sections. The two key steps in the proposed method are described in more details in Sections 2.3 and 2.4.

2.3. Constructing a complete inundation area-river stage relationship (IARSR) curve

According to Pan and Nichols (2013), there are three steps to construct the IARSR curve using DEM data. The first step is to define a polygon that covers the cross section where the IARSR is constructed. The width of the polygon should be significantly wide such that the polygon covers at least one side of the riverbanks plus a portion of the floodplain. The other side of the polygon should be at least 2-pixel-size of satellite images (used for measuring river inundation areas) long, which is about 60 m for the Landsat Thematic Mapper (TM) imagery.

The second step is to identify the minimum elevation inside the polygon. This minimum elevation actually represents the water surface elevation inside the polygon when the terrain survey was conducted or aerial photos were taken for producing the DEM data. All connected pixels with the same elevation as the minimum elevation (z_o) inside the polygon form the inundation area inside the polygon and the associated inundation area (A_o) is given by:

$$A_o = N \times D^2 \quad (13)$$

where N is the number of all connected pixels inside the polygon with the same elevation as z_o , and D is the grid cell size of the DEM data (usually each grid cell of the DEM data is a square, i.e., resolutions in x and y directions are the same). On the inundation area – river stage plane, the point (A_o, z_o) represents the lowest limit of the IARSR curve that can be derived from the DEM data (here 0 m is designated to be the reference level and thus the water surface elevation is also the river stage). Beneath this point, no terrain information can be extracted from the DEM data. Fig. 2a illustrates an example. The number labeled inside each grid cell stands for elevation. Inside the polygon (the red box), the minimum elevation is 7 m and there are 30 connected pixels with an elevation of 7 m, therefore, the lowest limit of the IARSR curve is $(30 \text{ m}^2, 7 \text{ m})$. Here the grid cell size of the DEM data shown in Fig. 2a is 1 m.

The third step is an iterative loop for obtaining multiple points for constructing the IARSR curve and these multiple points are all

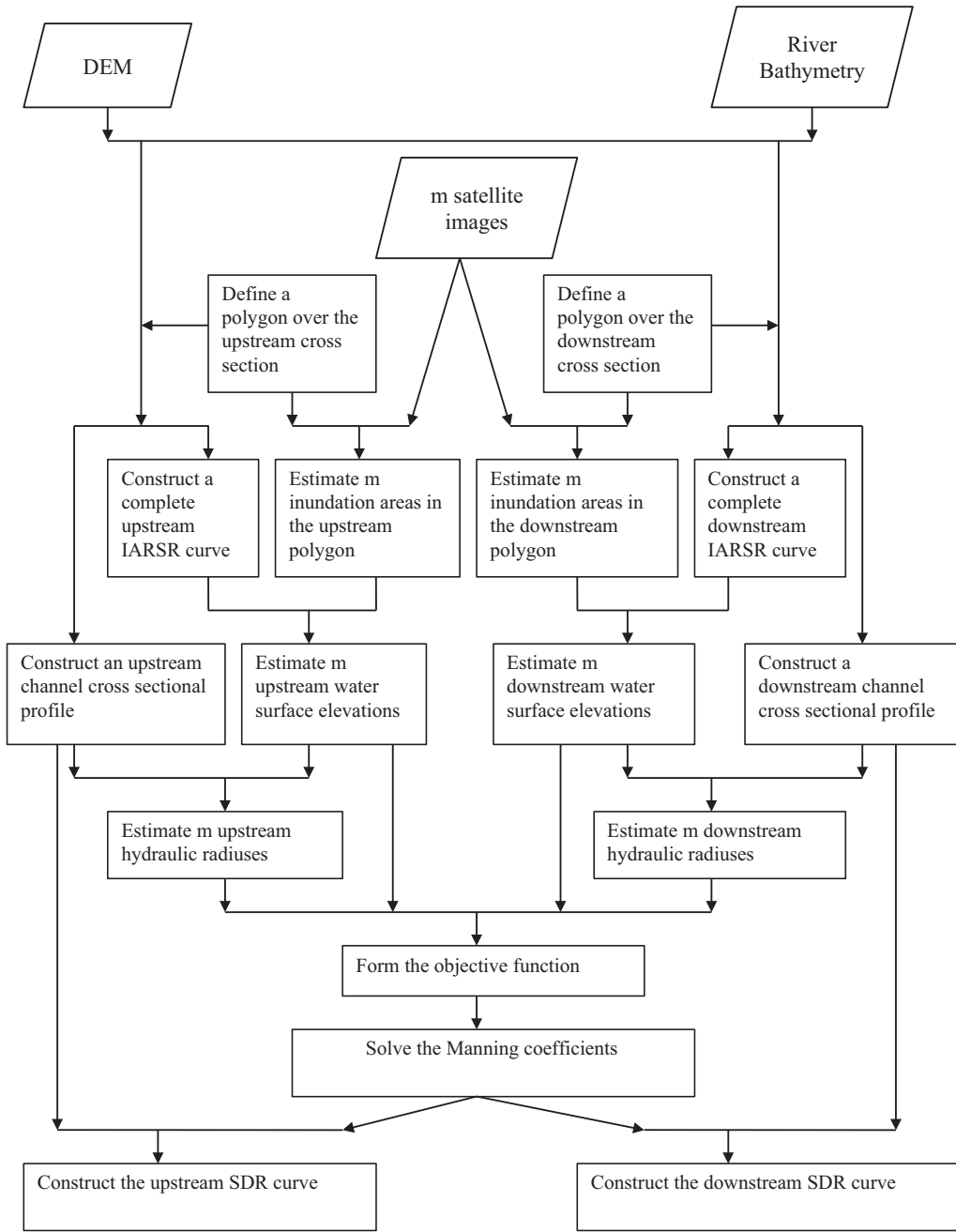


Fig. 1. Flow chart of the proposed method.

above the lowest limit point (A_o, z_o). To obtain points above (A_o, z_o), we can “artificially” raise the water level and use the hypothetical water level to determine the associated inundation area. As shown in Fig. 2a, when we set the water level at 8 m, the number of all connected submerged pixels (i.e., elevation ≤ 8 m) is 42, and thus the inundation area is 42 m^2 yielding another point ($42 \text{ m}^2, 8$ m) for constructing the IARSR curve. Using the same method, the other four points can be obtained inside the polygon: ($54 \text{ m}^2, 9$ m), ($66 \text{ m}^2, 10$ m), ($78 \text{ m}^2, 11$ m), ($90 \text{ m}^2, 12$ m). The IARSR curve can be constructed through best fitting these six points using a curve fitting method, e.g., the smoothing spline method (Pan and Nichols, 2013; and Pan et al., 2013). However, the constructed IARSR curve (Fig. 2b) based on the DEM shown in Fig. 2a is only applicable at river stages above the minimum water surface elevation detected by the DEM data, which is 7 m in this case. If a river bathymetric dataset is available, the channel bed elevation can be

extracted from the river bathymetry, i.e., subtracting the water surface elevation by the water depth. We then combine the DEM and the channel bed elevation, and obtain a new digital terrain model (DTM) dataset representing the solid surface elevation as shown in Fig. 2c. Using the same approach described above, we can obtain two more points: ($18 \text{ m}^2, 6$ m) and ($6 \text{ m}^2, 5$ m). Applying the smoothing spline method to fit eight points yields a complete IARSR curve starting from the channel bed (see Fig. 2d). Once a complete IARSR curve is constructed, it is straightforward to use the curve to estimate river stage from the satellite-measured inundation area (SMIA).

2.4. Constructing the stage-discharge rating (SDR) curve

To construct the stage-discharge rating (SDR) curve, m pairs of river stages or water surface elevations at both upstream and

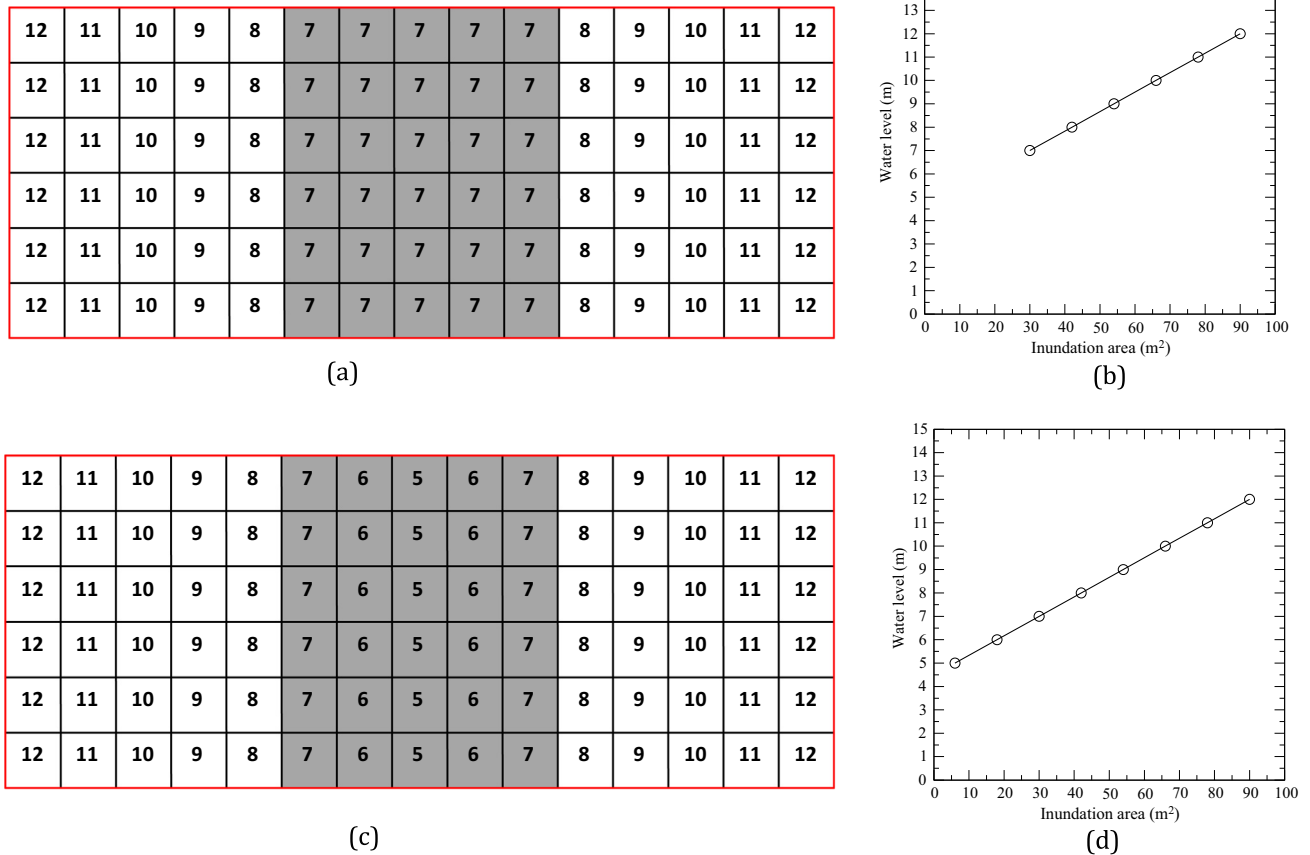


Fig. 2. Construct the inundation area-river stage relationship (IARSR) curve.

downstream cross sections are estimated from the satellite measured inundation areas. To produce inputs for the objective function Φ (i.e., Eq. (12)), the hydraulic radius associated with each river stage (or water surface elevation) needs to be estimated from the channel cross sectional profile. To determine the hydraulic radius, we first draw a line perpendicular to the river channel and passing through the center of the pre-defined polygon. Along this line, we can make a transect plot of the solid surface elevation. The hydraulic radius is computed as the ratio of the cross sectional area to the wetted perimeter. To compute the cross sectional area, we can use the trapezoidal rule. The detailed steps for estimating the hydraulic radius and the cross sectional area associated with a river stage or water surface elevation (z) can be described using Fig. 3 as an example. The first step is to determine the intersection

points between the water surface and the left or right riverbank. A line is drawn a to connect these two intersection points which is then equally divided into N segments. To achieve an accurate estimation, a small interval such as less than or equal to 1 m, is suitable. At each of the $N+1$ points a vertical line is drawn perpendicular to the water surface to produce $N+1$ intersection points along the channel bed. At points 0 and N , the point on the water surface coincides with the point on the channel bed since the water depth is zero at these two points. The linear interpolation method is used to estimate the coordinates (i.e., x, y, z) of each intersection point on the channel bed based on the solid surface elevation derived from DEM and river bathymetric data. Finally the cross sectional area is computed using the trapezoidal rule as follows:

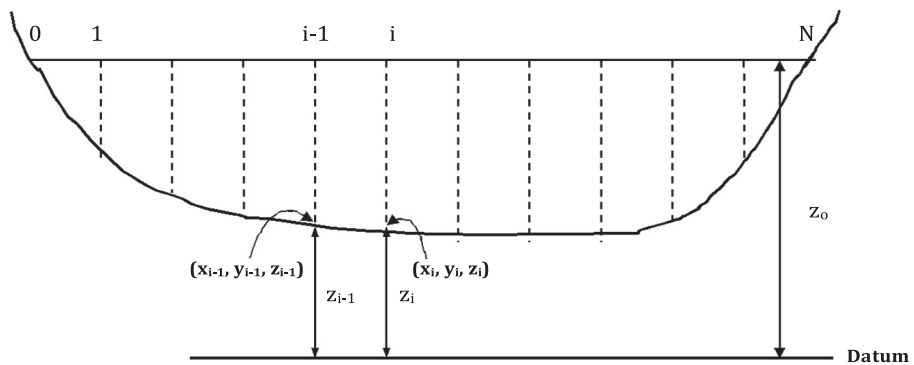


Fig. 3. Compute the cross sectional area using the trapezoidal rule.

$$A = \sum_{i=1}^N \{[(x_{i-1} - x_i)^2 + (y_{i-1} - y_i)^2]^{1/2} [(z_o - z_{i-1}) + (z_o - z_i)]/2\} \quad (14)$$

The hydraulic radius is calculated as below:

$$R = \frac{\sum_{i=1}^N \{[(x_{i-1} - x_i)^2 + (y_{i-1} - y_i)^2]^{1/2} [(z_o - z_{i-1}) + (z_o - z_i)]/2\}}{\sum_{i=1}^N [(x_{i-1} - x_i)^2 + (y_{i-1} - y_i)^2 + (z_{i-1} - z_i)^2]^{1/2}} \quad (15)$$

3. Study area and data

The river reach between two USGS gauging stations along the lower Illinois River is selected as the study area (Fig. 4), because a high quality (error ± 12 cm) and 5-m horizontal resolution channel bathymetry raster dataset developed by the Upper Midwest

Environmental Sciences Center (UMESC) of the USGS (Rogala, 1999) is available over the study area. The upstream gauging station is at Kingston Mines (USGS 05568500) (hereafter KM site), and the downstream gauging station is at Copperas Creek (USGS 05568615) (hereafter CC site) (Fig. 4). The geographic information, gauge datum, drainage area, and start and end dates of river discharge and stage height measurement of each site are listed in Table 1. The reach length between these two stations is 14,897 m. The riverbed slope in this reach is very gentle and the average bed slope for the lower Illinois River is only about 1.6 inches per mile or 0.000025 m/m (Bhowmik and Schicht, 1979; Bhowmik and Soong, 2000).

A 1/9 arc-second digital elevation model (DEM) dataset with a horizontal resolution of about 3 m (Gesch et al., 2002; Gesch, 2007) was obtained from the National Elevation Database (NED). To match the projection and horizontal resolution between the UMESC channel bathymetry raster dataset over the La Grange Pool and the downloaded DEM data, both DEM and bathymetry raster

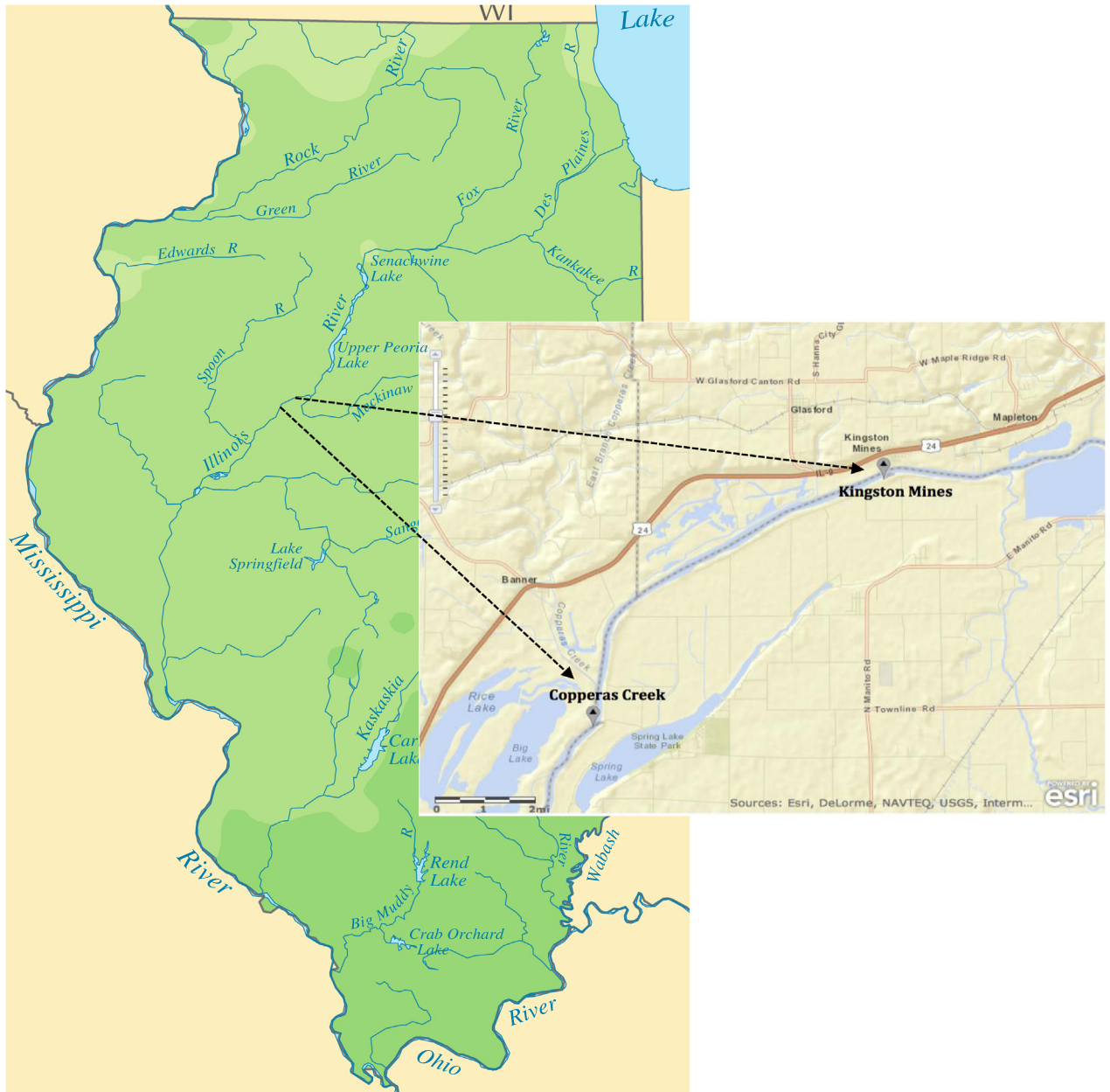


Fig. 4. A river reach along the Illinois River between the upstream USGS station at Kingston Mines (KM) and the downstream USGS station near Copperas Creek (CC).

Table 1

Two USGS gauging stations along the Illinois River.

Station	Latitude	Longitude	Gage datum (NAVD88)	Drainage area	Discharge measurement Start date–End date	Gage height measurement Start date–End date
Kingston mines	40°33'11"	89°46'38"	130.352 m ^a	40,968 km ²	1939/10/1 – current	1993/10/1 – current
Copperas creek	40°28'34"	89°53'18"	130.349 m ^a	39,860 km ²	NA	1993/10/1 – current

^a Gage datum was converted from NGVD29 to NAVD88 for matching the DEM data.

datasets were re-projected to the Universal Transverse Mercator (UTM) projection (zone 16), and re-sampled to 3 m using the ArcGIS cubic convolution interpolation method. The re-projected and re-sampled DEMs are shown in Figs. 5a and 6a. The locations of KM site and CC site are marked on Fig. 5a and 6a, respectively.

As discussed in Section 2, channel bed elevation is needed to construct a complete IARS curve in a pre-defined polygon. In this study, the UMESC river bathymetry dataset developed in 1997 was used to determine the channel bed elevation through subtracting the reference water surface elevation, which is 429 ft or 130.7592 m (Rogala, 1999), by the water depth (i.e., bathymetry) at each UMESC river bathymetry raster grid. Then the elevation values of these grids in the DEM were replaced by the computed channel bed elevations and shown in Figs. 5b and 6b. According to Fig. 6b, there were no bathymetric measurements over the CC

site and the surrounding area, therefore a polygon covering a downstream area where bathymetric information was available was selected and illustrated in Fig. 6b. The distance from the center of the polygon to the CC site is about 750 m. For such short distance, we assume that the bathymetry and water level variation between the CC site and the center of this polygon is negligible. The pre-defined polygon over the KM site is shown in Fig. 5b.

Since the DEM and bathymetric data are from two different sources and ground survey times for collecting data to produce DEM and bathymetric data could not be the same, and thus the water surface elevation in the DEM does not match that in the UMESC bathymetric data. As a result, a simple direct combination of the DEM and the channel bed elevation could produce a discontinuity in the elevations at the boundary between pixels with and without bathymetric information. To illustrate this problem, a

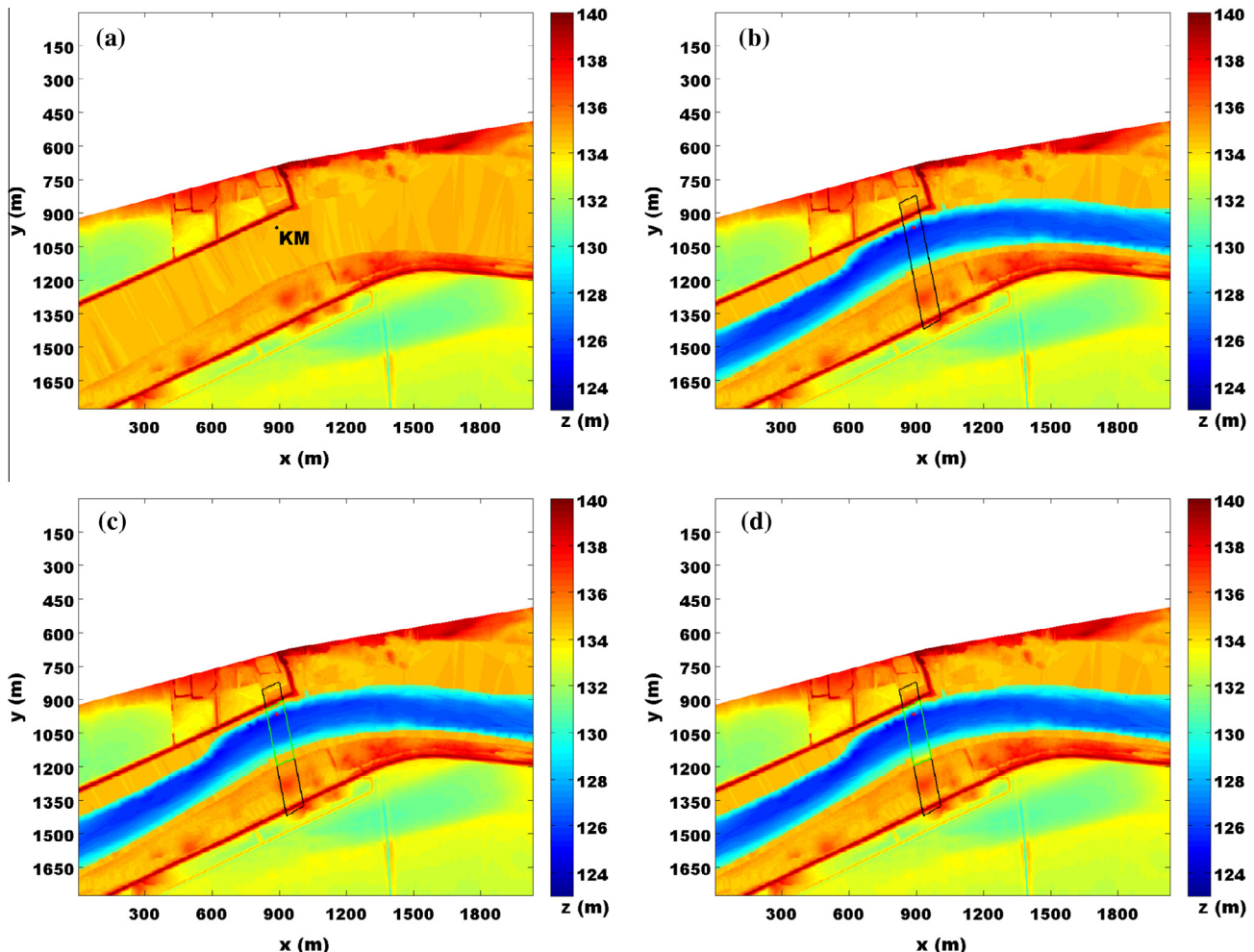


Fig. 5. (a) DEM at KM site and in the surrounding area. (b) Combined DEM and riverbed elevation. The pre-defined polygon covering KM site is shown as the black polygon (black). (c) Linear interpolation is performed to eliminate the discontinuity between the DEM and riverbed elevation inside the discontinuous zone (green polygon). (d) New combined DEM and riverbed elevation after the discontinuity was removed. (For interpretation of the references to colour in this figure legend, the reader is referred to the web version of this article.)

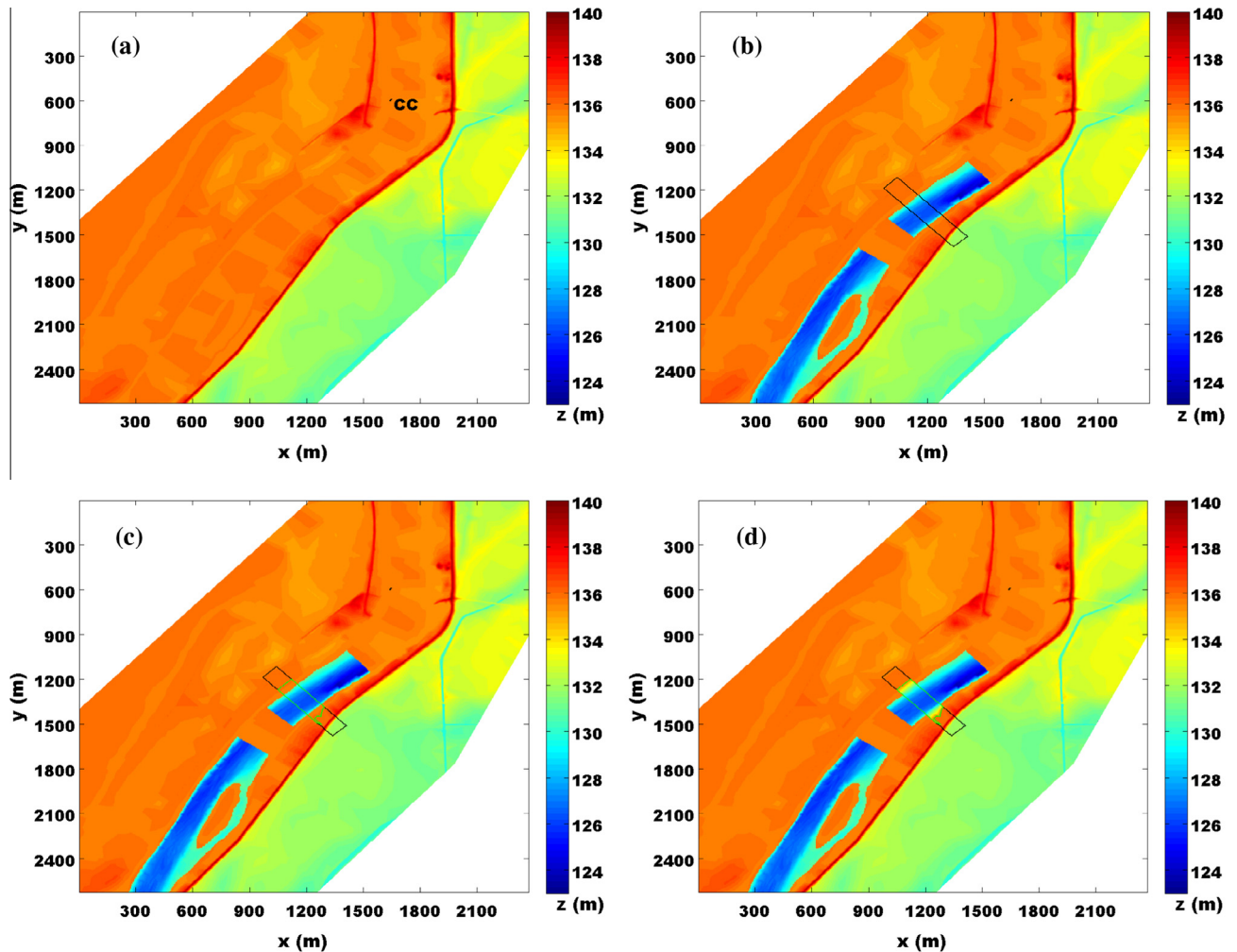


Fig. 6. (a) DEM at CC site and in the surrounding area. (b) Combined DEM and riverbed elevation. Since no river bathymetric measurement is available surrounding CC site, a polygon (black) at a distance of 750 m downstream from CC site is selected. (c) Linear interpolation is performed to eliminate the discontinuity between the DEM and riverbed elevation inside the discontinuous zone (green polygon). (d) New combined DEM and riverbed elevation after the discontinuity was removed. (For interpretation of the references to colour in this figure legend, the reader is referred to the web version of this article.)

transect plot of elevations along the central line passing the center of each pre-defined polygon is drawn in Fig. 7. In order to eliminate this discontinuity, we used the linear interpolation method to calculate the elevation in the discontinuous zones (green boxes in Figs. 5c and 6c) and plotted the new elevations in Figs. 5d and 6d. The transect plots of the re-calculated elevations shown in Fig. 7 indicate that the linear interpolation is effective in eliminating the discontinuity in the channel bed elevation profiles.

To determine the mean channel bed slope in the study area (i.e., the reach between KM and CC sites), we sampled 84 lowest channel bed elevations along the reach using the bathymetry data to construct the thalweg. A scatter plot of the thalweg points versus the distance from the upstream site (i.e., KM site) is shown in Fig. 8. The slope of the best-fit line of the scatter plot is about 0.00005 (m/m), which is about twice the average bed slope of the lower Illinois River (Bhowmik and Schicht, 1979; Bhowmik and Soong, 2000).

Landsat 5 Thematic Mapper (TM) satellite band 5 images were obtained from the USGS Earth Resources Observation and Science (EROS) data center. According to Overton (2005), in band 5 (1.55–1.75 μm, mid-infrared) water has a very low reflectance and soil and vegetation on dry land have very high reflectance, therefore a sharp contrast between water and dry areas under

the clear-sky condition is often visible on the Landsat TM band 5 images. 47 Landsat band-5 images collected during 1994–2002 with clear sky over the study area were used in this study and the date of each image is listed in Table 2.

4. Results and discussion

4.1. Estimate river water surface elevation

The accuracy of the estimated inundation areas directly influences the accuracy of the estimated water surface elevations. To reduce the uncertainty in the estimated inundation areas, Pan and Nichols (2013) proposed a dual-threshold method to determine fully and partially flooded pixels. The first threshold is the lower limit of pixel value for classifying water body pixels with a relatively high-level certainty. The second threshold is the upper limit of pixel value for classifying potentially flooded pixels. All pixels with values between the first threshold and the second threshold and adjacent to the classified water body pixels may be partially flooded. A linear interpolation method was used to estimate the wetted area of each partially flooded pixel. Similar to the dual-threshold method, we actually can first resample Landsat imagery from the 30-m resolution to a finer resolution (i.e., 3 m

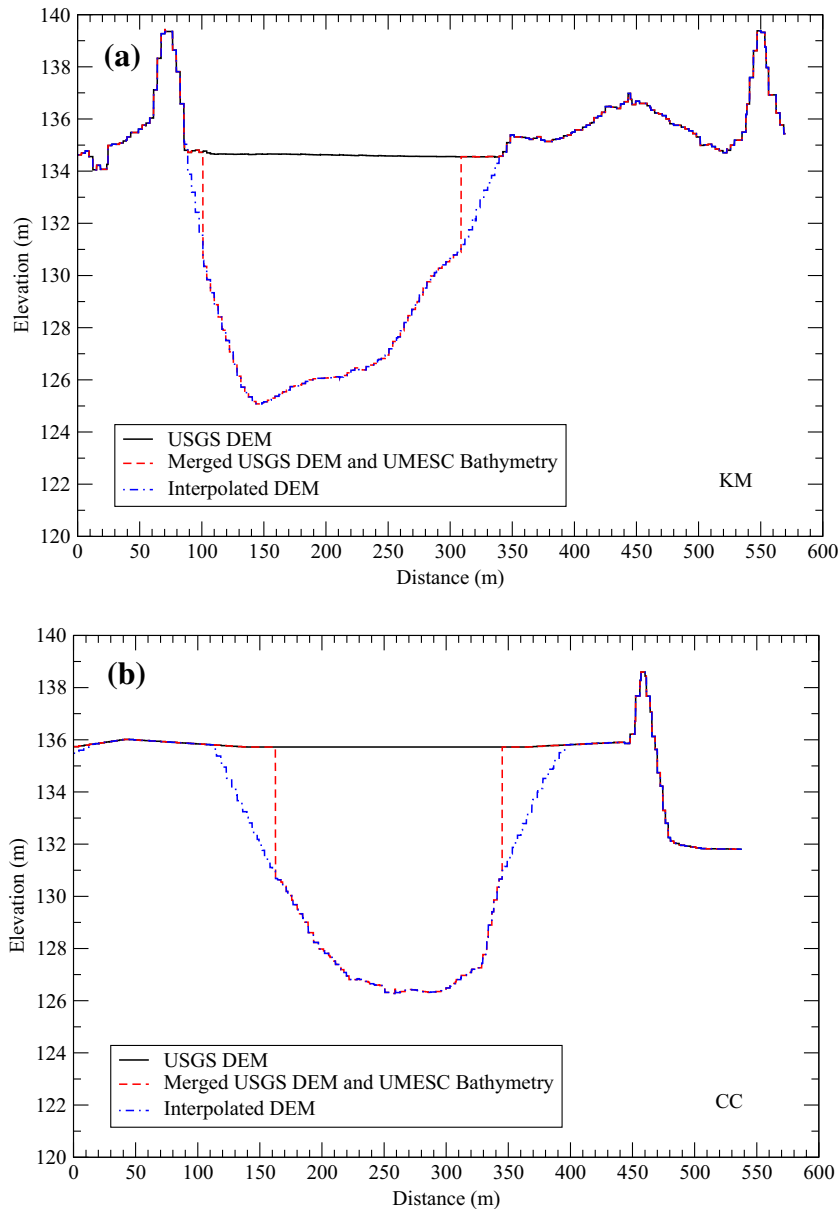


Fig. 7. Transect of elevation at (a) KM site and (b) CC site.

in this study, since the resolution of the DEM data used in this study is 3 m) using the cubic convolution interpolation method because of its high accuracy (Keys, 1981) and then we can directly use the single-threshold or density slice method (also known as the image histogram thresholding method) (e.g., Frazier and Page, 2000; Brivio et al., 2002; Matgen et al., 2004; Overton, 2005; Smith and Pavelsky, 2009) to determine flooded pixels.

After resampling Landsat imagery from 30-m to 3-m resolution, using a single threshold to determine the boundary between water body and dry riverbanks in the pre-defined polygon over a river cross section may still have some uncertainties, because there are two riverbanks (left side and right side) at a river cross section and each side may have different slopes and thus the threshold for separating water and dry-land pixels may be different between right and left riverbanks. To eliminate the uncertainty due to slope differences, we defined a small polygon inside the pre-defined polygon to only cover the north side of the riverbank and a portion of river channel (see Fig. 9) at KM or CC site, because both USGS gauging stations at KM and CC sites are located on the north side

of the Illinois River. The re-defined smaller polygons at KM and CC sites were used to construct the IARSR curves and estimate water surface elevations.

Using the method described in Section 2, we first constructed the IARSR inside the re-defined polygons at KM and CC sites. The data points (i.e., inundation area versus water surface elevation) at KM and CC sites are plotted in Fig. 10. The smoothing spline curve fitting method (embedded in the Matlab curve fitting toolbox) was then used to best fit these data points to obtain the IARSR curves inside the re-defined polygons. The best-fit IARSR curves are also shown in Fig. 10. Since the smoothing spline curve fitting method does not produce any analytical expressions, we used Matlab to evaluate the water surface elevations at different inundation areas with a small area increment (e.g., 9 m²) and export as a data file of the IARSR curve. When we use the IARSR to estimate water surface elevation from the satellite measured inundation area (SMIA), we first search the IARSR curve data file to find two points IA_i and IA_{i+1} satisfying the following condition:

$$IA_i < SMIA \leq IA_{i+1} \quad (16)$$

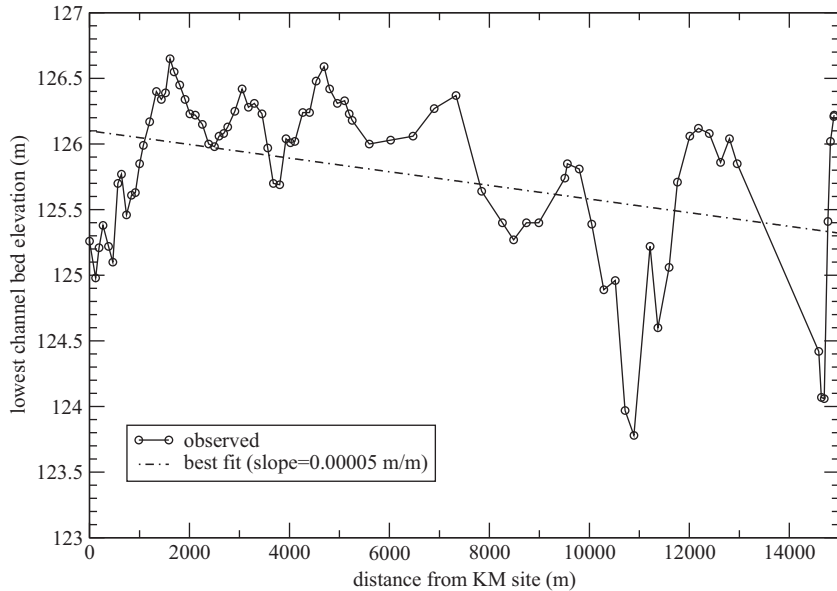


Fig. 8. Transect of the lowest channel bed elevations between KM and CC sites.

Then the water surface elevation is computed as follows:

$$z = z_i + \frac{(SMIA - IA_i)}{(IA_{i+1} - IA_i)} (z_{i+1} - z_i) \quad (17)$$

Even just determining one single threshold for identifying the boundary between water body and dry riverbank is not a simple task because, at times, there may not be a distinct valley between two peaks (one peak is associated with water pixels, and the other peak is related to dry land pixels) on the histograms of the Landsat images. Under such conditions, visual inspection is necessary for determining the water-dry riverbank boundary. To help the visual inspection of the boundary, we computed the Landsat band 5 image digital number (DN) gradient along a line through the center of the defined polygon (for example, the red line in Figs. 11 and 12). The DN profile along this line runs from the riverbank toward the river channel and is plotted in Fig. 11 for KM site and Fig. 12 for CC site. The Matlab smoothing spline curve fitting method is used to best fit the DN profiles. Similar to constructing the IARSR curve, a data file of the best-fit DN profile is generated through evaluating DN values at different pixel distances (PDs) with a small distance interval (e.g., 0.1). The DN gradient (DNG) is computed as follows:

$$DNG_i = \frac{DN_{i+1} - DN_{i-1}}{PD_{i+1} - PD_{i-1}} \quad (18)$$

The DNG profiles shown in Figs. 11 and 12 reveal a minimum of the DN gradient corresponding to the water-dry riverbank boundary. The DN at this DNG minimum is the threshold for separating water and dry-land pixels. With the combination of the image histogram thresholding method, DN gradient profile, and visual inspection, we first determined the threshold, and then we computed the number of pixels inside the defined polygon with DNs less than or equal to the threshold. The inundation area is equal to the number of wetted pixels multiplied by the grid cell area, which is 9 m² in this study.

Table 2 lists 47 estimated inundation areas and the associated thresholds at each site from 47 Landsat images. Using the constructed IARSR curves, we estimated water surface elevations corresponding to these estimated inundation areas at KM and SC sites. Both estimated and observed water surface elevations at

these two sites are also listed in Table 2. The root mean square errors (RMSEs) and the correlation coefficients (*r*) between the estimated and observed water surface elevations are: RMSE = 0.05 m, *r* = 0.999 at KM site, and RMSE = 0.04 m, *r* = 0.999 at CC site. Small errors and high correlation coefficients indicate that the proposed method to estimate water surface elevation (or river stage) is robust.

4.2. Construct stage-discharge rating curves

After obtaining 47 water surface elevations at both KM and CC sites, we estimated the corresponding hydraulic radii using the method described in Section 2.4. We then substituted 47 estimated water surface elevations and the associated hydraulic radii at KM and CC sites into the objective function Φ (i.e., Eq. (12)). As shown in Section 3 and Fig. 8, the estimated reach average channel bed slope is 0.00005 m/m, and the reach length is about 14,897 m. In this study, we used the nonlinear global optimization function embedded in Mathematica (i.e., NMinimize) based on the Nelder-Mead method (Nelder and Mead, 1965) to solve four parameters (i.e., α , n , b , and k_L) for minimizing the objective function Φ given in Eq. (12). Constraining the four parameters as: $1 \leq \alpha \leq 1.5$, $0 < n \leq 0.05$, $b > 0$, $0 \leq k_L \leq 1$, yielded: $\alpha = 1.04$, $n = 0.027$, $b = 0.216$, and $k_L = 1$. The minimum of the objective function Φ is 0.33 (m²).

With the solved optimal Manning's coefficient, we can construct the SDR curves at both upstream and downstream sites. However, no discharge data are available at CC site, therefore, the validation of the constructed SDR curves was only carried out at the KM site. To establish the SDR curve at the KM site, we applied the solved Manning's coefficient and the Manning's equation to compute river discharges at a series of water surface elevations from the lowest channel bed elevation to the bank-full level, which is about 135.38 m at the KM site, because this study only focuses on the main channel flow and the overbank flow is beyond the scope of this study. The constructed SDR curve is plotted in Fig. 13 along with the scatter plot of 47 river water surface elevation versus discharge data points measured by the USGS gauging station at the KM site during the same days as the Land-

Table 2

Dates of Landsat images and estimated inundation areas and water surface elevations.

Year	Month	Day	KM site			CC site		
			Threshold	A (m ²)	z (m)	z* (m)	Threshold	A (m ²)
1994	3	15	50	8505	135.30	135.21	44	14,112
1994	3	31	43	8217	133.82	133.84	39	12,942
1994	5	18	58	8172	133.60	133.65	36	12,861
1994	5	27	59	7848	132.11	132.11	39	11,538
1994	6	19	44	7992	132.75	132.70	39	11,970
1994	7	5	62	7839	132.07	132.05	29	11,538
1994	8	22	45	7839	132.07	132.10	40	11,565
1994	10	9	50	7668	131.33	131.31	30	10,908
1994	11	10	42	8190	133.69	133.70	32	12,879
1994	11	26	36	7929	132.47	132.48	32	11,826
1995	5	5	46	8451	135.02	134.98	42	13,914
1995	6	22	60	8334	134.42	134.37	40	13,455
1995	7	1	52	8199	133.74	133.66	42	12,888
1995	7	17	54	7812	131.95	131.95	34	11,466
1995	8	9	43	7992	132.75	132.81	34	12,105
1995	8	18	55	7893	132.31	132.32	33	11,745
1995	8	25	43	7839	132.07	132.13	32	11,619
1995	9	3	42	7704	131.50	131.43	31	11,070
1995	9	10	43	7758	131.73	131.69	36	11,277
1995	10	12	45	7668	131.33	131.27	30	10,854
1996	4	21	53	7893	132.31	132.33	52	11,691
1997	3	23	56	8487	135.20	135.20	34	14,103
1997	5	10	60	8154	133.52	133.53	40	12,663
1997	7	13	58	7848	132.11	132.18	49	11,664
1997	7	29	51	7956	132.59	132.54	37	11,907
1997	9	15	40	7695	131.46	131.43	40	11,061
1997	10	1	63	7686	131.42	131.42	36	10,935
1997	11	18	52	7713	131.54	131.41	35	10,827
1998	9	2	61	7740	131.65	131.67	48	11,187
1998	9	18	49	7722	131.58	131.49	35	11,070
1998	10	20	53	7983	132.71	132.79	28	12,078
1998	11	21	37	7821	131.99	132.01	33	11,475
1999	3	29	44	8127	133.39	133.33	41	12,546
1999	6	17	54	8514	135.35	135.35	52	14,139
1999	8	29	38	7722	131.58	131.61	31	11,151
2000	2	12	54	7677	131.38	131.43	40	10,998
2000	5	2	48	8181	133.65	133.71	39	12,834
2000	9	7	62	7632	131.16	131.09	46	10,701
2000	10	9	48	7758	131.73	131.67	35	11,223
2001	3	18	52	8406	134.80	134.79	48	13,851
2001	9	10	65	7758	131.73	131.67	38	11,214
2001	9	26	49	7965	132.63	132.66	34	12,033
2001	10	28	47	8388	134.71	134.68	38	13,680
2002	1	25	43	7812	131.95	131.87	37	11,448
2002	8	28	44	8154	133.52	133.45	37	12,636
2002	9	6	49	7686	131.42	131.34	33	10,980
2002	9	29	43	7650	131.25	131.21	37	10,773

Threshold is used for separating water and dry-land pixels. A is the estimated inundation area inside the pre-defined polygon, z is the estimated water surface elevation based on the constructed IARSR curve and estimated inundation area, and z* is the USGS measured water surface elevation at the gauging stations.

sat images were taken. The root mean square error (RMSE) and the correlation coefficients (*r*) between the estimated and USGS measured river discharges are RMSE = 112.4 m³/s and *r* = 0.95, respectively.

By inspecting the constructed SDR curve shown in Fig. 13, we can find that the constructed SDR curve tends to overestimate discharge under low flow conditions and underestimate discharge under high flow conditions. The main reason is that we used only one Manning's coefficient for estimating river discharge in the entire dynamic range of water surface elevation from the lowest channel bed elevation to the bank-full level. For a wide channel, as water level is very low and close to the lowest channel bed elevation, the impact of channel bed roughness on flow should be much greater than the impact of channel bed roughness on flow as water level is at the bank-full level. Therefore, as water level increases and approaches to the bank-full level, the Manning's coefficient should decrease. Once the water level above the bank-full level, overbank flow occurs and the Manning's coefficient could

either increase or decrease, which depends on the floodplain roughness. But in the main channel as water level is less than or equal to the bank-full level, we can use a power-law function to describe the vertical decline of the Manning's coefficient as follows:

$$n = n_B \left[1 - \left(1 - \frac{n_{BF}}{n_B} \right) \left(\frac{z - z_o}{z_{BF} - z_o} \right)^c \right] \quad (19)$$

where *n_B* and *n_{BF}* are the Manning's coefficients at the lowest channel bed elevation and the bank-full level, respectively, *z_o* is the lowest channel bed elevation, *z_{BF}* is the bank-full water surface elevation, and *c* is a constant greater than 1. The Manning's coefficients at the lowest channel bed elevation *n_B* should be greater than the determined single Manning's coefficient *n* in Eq. (12), which is 0.027, while the Manning's coefficients at the bank-full level *n_{BF}* should be less than 0.027. Substituting Eq. (19) into the objective function *Φ* given in Eq. (12), yields:

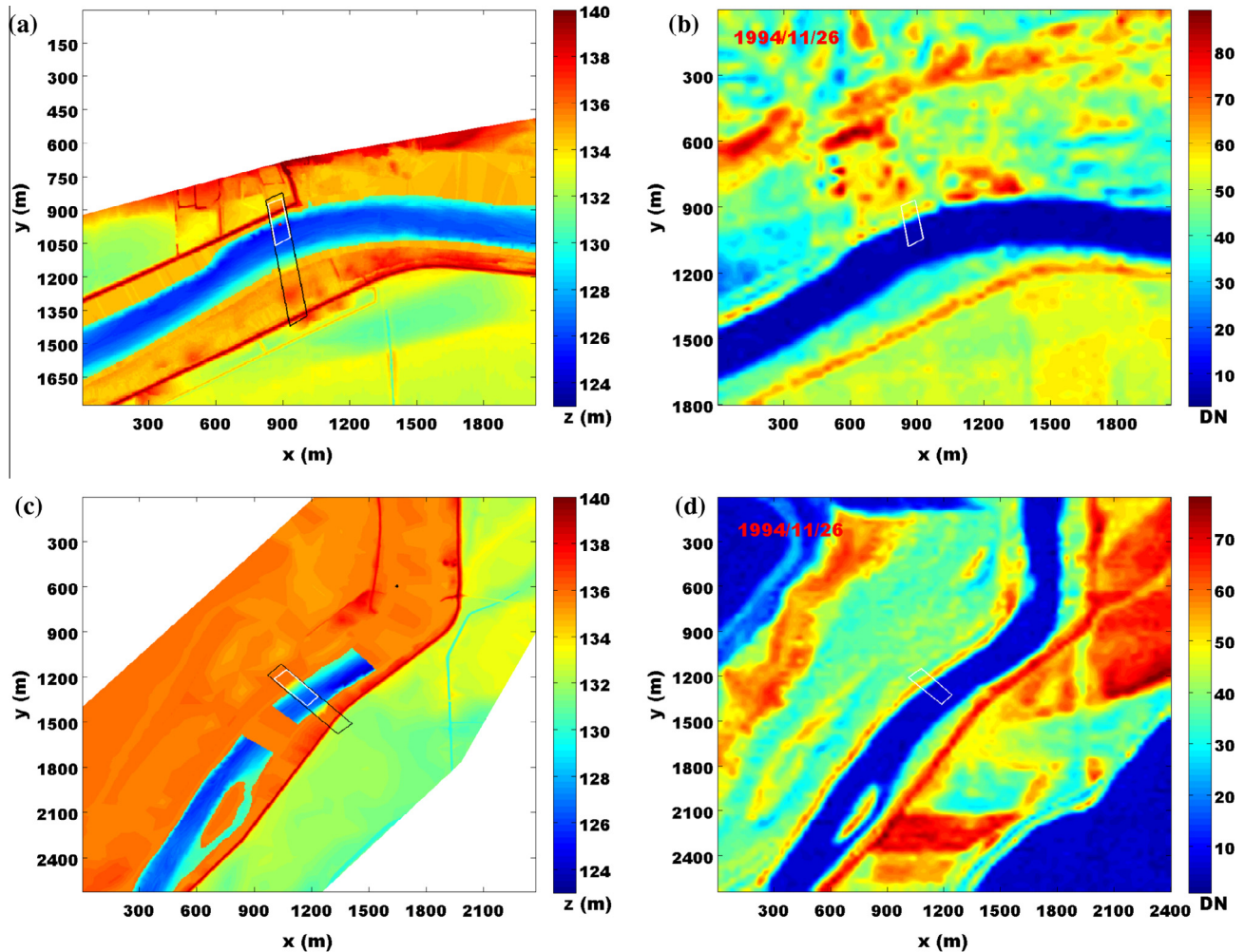


Fig. 9. (a) Elevation, the IARSR curve is constructed inside the smaller polygon (white box) inside the pre-define polygon at KM site. (b) Landsat band 5 image over KM site on 1994/11/26. (c) Elevation, the IARSR curve is constructed inside the smaller polygon (white box) inside the pre-define polygon at CC site. (d) Landsat band 5 image over CC site on 1994/11/26.

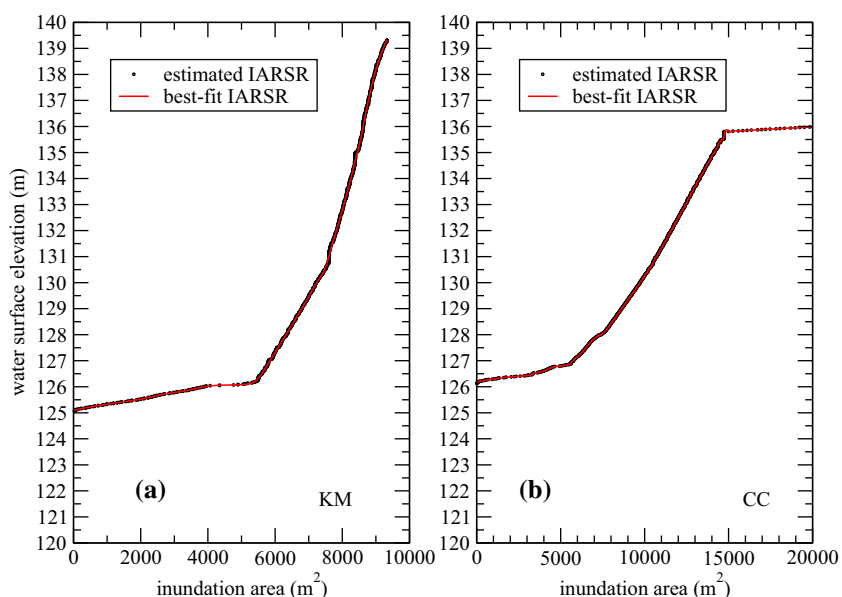


Fig. 10. Estimated and best-fit IARSR curve (a) at KM site (b) at CC site.

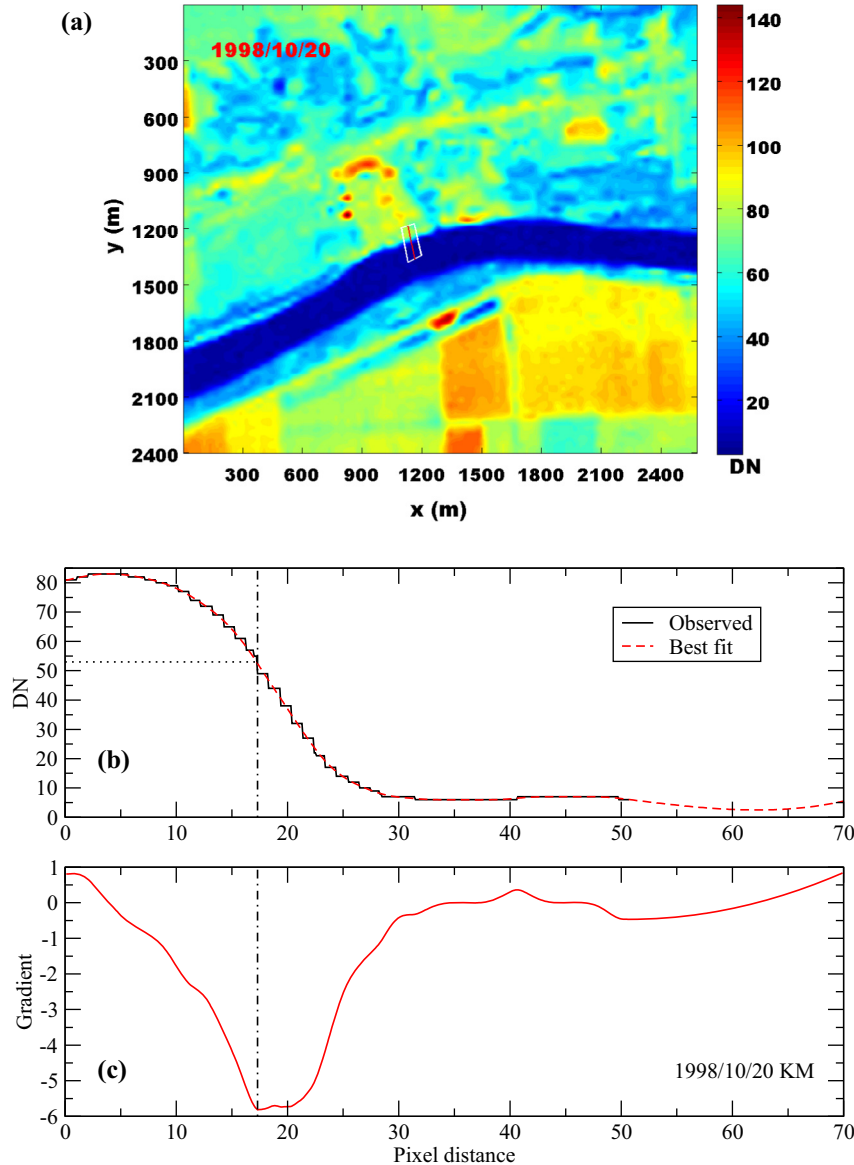


Fig. 11. (a) Landsat image over KM site on 1998/10/20. (b) Observed and best-fit pixel digital number profiles along the central line passing through the pre-defined polygon. (c) Landsat image pixel DN gradient profile along the central line passing through the pre-defined polygon.

$$\Phi = \sum_{i=1}^m \left\{ z_{1i} + \alpha \frac{R_{1i}^{4/3} b S_b}{2gn_B^2 \left[1 - \left(1 - \frac{n_{BF}}{n_B} \right) \left(\frac{z_{1i} - z_{o1}}{z_{BF1} - z_{o1}} \right)^c \right]^2} - z_{2i} - \alpha \frac{R_{2i}^{4/3} b S_b}{2gn_B^2 \left[1 - \left(1 - \frac{n_{BF}}{n_B} \right) \left(\frac{z_{2i} - z_{o2}}{z_{BF2} - z_{o2}} \right)^c \right]^2} - b S_b L - k_L \left| \alpha \frac{R_{1i}^{4/3} b S_b}{2gn_B^2 \left[1 - \left(1 - \frac{n_{BF}}{n_B} \right) \left(\frac{z_{1i} - z_{o1}}{z_{BF1} - z_{o1}} \right)^c \right]^2} - \alpha \frac{R_{2i}^{4/3} b S_b}{2gn_B^2 \left[1 - \left(1 - \frac{n_{BF}}{n_B} \right) \left(\frac{z_{2i} - z_{o2}}{z_{BF2} - z_{o2}} \right)^c \right]^2} \right|^2 \right\} \quad (20)$$

Based on the channel cross sectional profile shown in Fig. 7, the bank-full flow depth at the KM site is about 10.31 m, and the lowest channel bed elevation is 125.07 m. Near the CC site, the bank-full flow depth is 9.52 m, and the lowest channel bed elevation is 126.28 m. Using the Mathematica's NMinimize function with the

following constrains: $1 \leq \alpha \leq 1.5$, $b > 0$, $n_B > 0.027$, $0 < n_{BF} < 0.027$, $c > 1$, $0 \leq k_L \leq 1$, we determined the six unknowns (i.e., α , b , n_B , n_{BF} , c , and k_L) in the objective function Φ which yielded the following results: $\alpha = 1.23$, $b = 0.216$, $n_B = 0.046$, $n_{BF} = 0.023$, $c = 1.1$, and $k_L = 1$. The associated minimal value of the objective function Φ is 0.32 m^2 . The constructed SDR curve using the solved n_B , n_{BF} and c is also plotted in Fig. 13. The root mean square error (RMSE) and the correlation coefficients (r) between the estimated river discharge using the constructed SDR curve and the USGS measured river discharges are RMSE = $83.9 \text{ m}^3/\text{s}$ and $r = 0.95$, respectively. According to Fig. 13, using the vertical profile of the Manning's coefficient as given in Eq. (19) improved the agreement between the observed and estimated river discharges.

4.3. Discussion

Since the proposed method in this study utilizes three types of data: DEM, river bathymetry, and Landsat TM imagery, the errors and uncertainties associated with these three types of data directly contribute to the errors in the constructed SDR curves. If finer

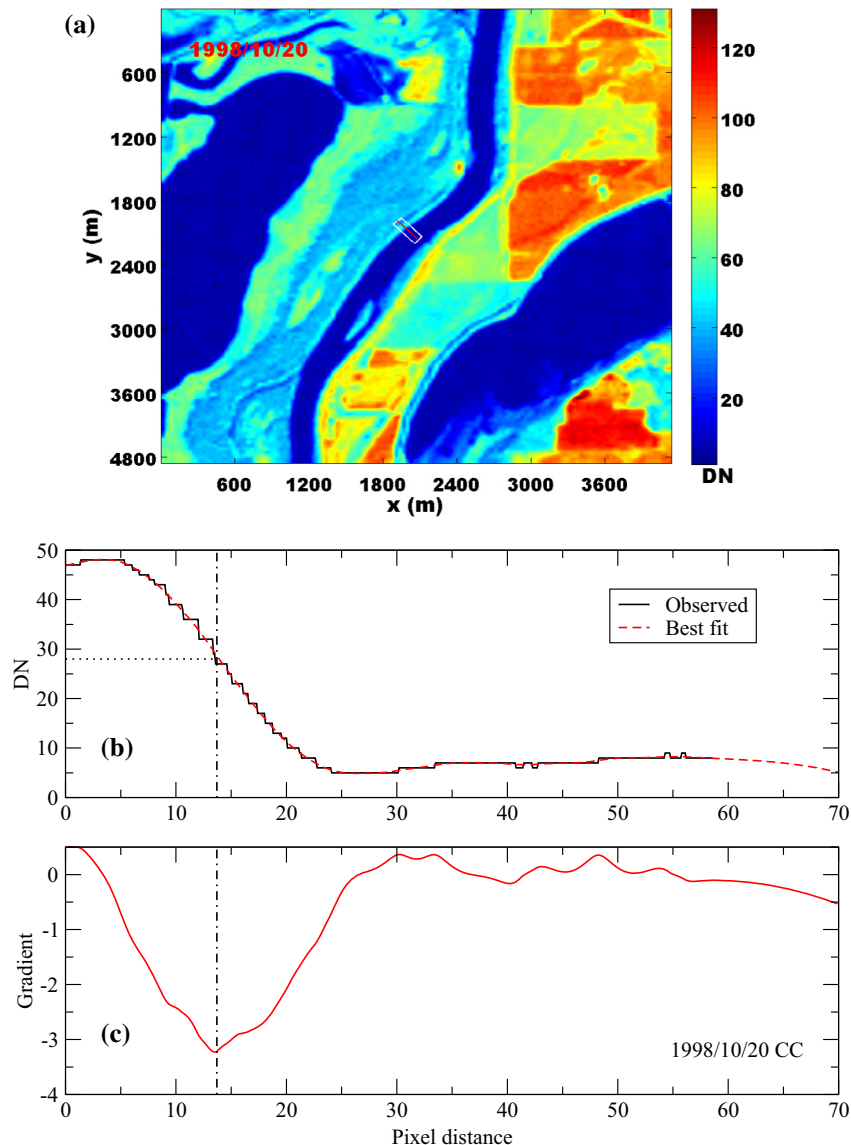


Fig. 12. (a) Landsat image over CC site on 1998/10/20. (b) Observed and best-fit pixel digital number profiles along the central line passing through the pre-defined polygon. (c) Landsat image pixel DN gradient profile along the central line passing through the pre-defined polygon.

resolution DEM and river bathymetric data (e.g. 1 m resolution lidar data) were available, more accurate IARSR would be obtained. This would result in improved accuracy of the estimated water surface elevation from the constructed IARSR. This is also true if higher resolution satellite images (e.g., QuickBird, WorldView, and GeoEye) were used to estimate inundation area. The effects of the horizontal resolutions of the DEMs and satellite images on the estimated water surface elevation using the proposed approach also depends on channel width and river bank slope, that is, for a narrow channel or a steep river bank slope, fine resolution DEM and satellite images need to be used. In this study, the bathymetry was developed in 1997, while our study period is from 1994 to 2002. During this period the bathymetry could change, which could also cause some errors in the constructed SDR curves.

Another error source might come from neglecting the lateral inflow in the Bernoulli equation (i.e., Eq. (3)). To ensure the valid assumption of insignificant lateral inflow in the energy balance equation, we would need to select a downstream site as close as possible to the upstream site. However, if the downstream site is too close to the upstream site, the difference in water surface

elevations between these two sites might be less than the errors in the estimated water surface elevations and thus can induce uncertainty and singularity in solving the Manning's coefficient using the nonlinear global optimization method. Therefore, an optimal reach length might exist for achieving the most accurate Manning's coefficient, which deserves a future systematic study.

The method developed in this study is based on the Bernoulli equation of gradually varied open channel flow along a river reach. The slope of the energy line is assumed to be the channel bed slope multiplied by a coefficient. However, flow in natural channels cannot always be steady and uniform, or gradually varied. Therefore, the traditional SDR curve approach to treat river discharge as a single function of river stage is subjected to errors and uncertainties, especially as the flow in natural channels greatly departs from a steady uniform flow. Under the rapidly varied and non-uniform flow condition, the relation between stage and discharge needs to be modified by some factors that can cause changes in the shape and position of the rating curve (Kennedy, 1984; Herschy, 1995; Rantz et al., 1982b; Braca, 2008). These factors include channel cross section change due to scour and fill, aquatic vegetation,

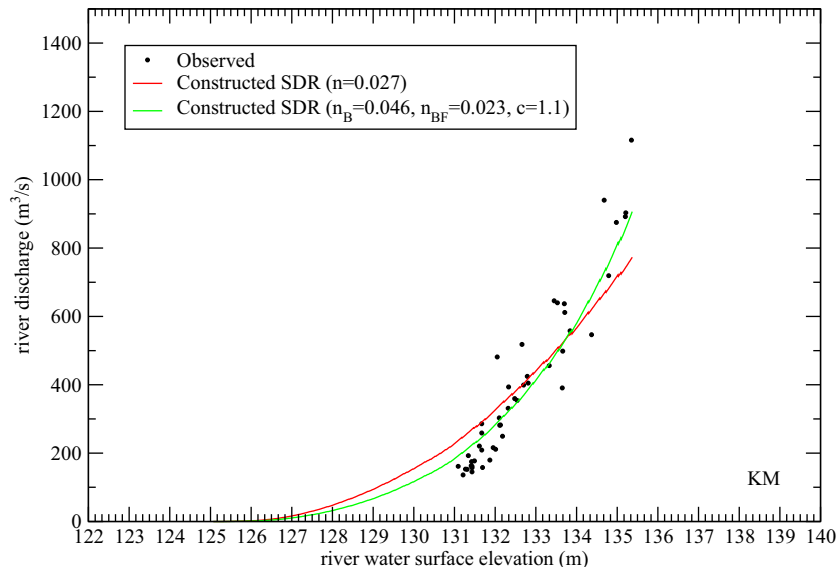


Fig. 13. Scatter plot of the USGS observed river discharge versus water surface elevation at KM site and the constructed SDR curves.

debris and log jams, backwater, rapidly varied discharge, discharge to or from overbank areas, and ice in channels (Braca, 2008).

One major limitation in our proposed method is the requirement of river bathymetry, because river bathymetry data are still very limited and not widely available. However, unlike river bathymetry, the National Oceanic and Atmospheric Administration (NOAA) and other research institutes have been spending tremendous effort in mapping ocean basin terrain and bathymetry of some major lakes in North America (e.g., Smith and Sandwell, 1997; Jakobsson et al., 2008; Becker et al., 2009). Here we would like to suggest more effort and research be carried out to survey river bathymetry and river channel geometry. As more river bathymetric data become available, our ability to measure river discharge at any ungauged cross section from space will be greatly improved. The requirement of high resolution of DEM data (e.g., 3-m resolution DEM used in this study) is another possible limitation, especially in developing countries. One possible solution is to utilize a ground-based scanning lidar to measure terrain for producing some high resolution DEM data over the cross sections where the SDR curves will be constructed. We also suggest more effort be carried out to improve the resolution of global DEM.

5. Summary

The goal of this study was to develop a new approach to construct the river stage-discharge rating (SDR) curves using remotely sensed river inundation areas and river bathymetry. The proposed method was tested over a river reach between two USGS gauging stations, i.e., Kingston Mines (KM) and Copperas Creek (CC), along the lower Illinois River where river bathymetric information is available from the Upper Midwest Environmental Sciences Center (UMESC) of the USGS. First a polygon over each of two cross sections (i.e., KM and CC sites) was defined. A complete inundation area – river stage relationship (IARSR) curve was constructed inside each polygon using the DEM and river bathymetric data. The constructed IARSR curves were then used to estimate 47 river water surface elevations at each cross section based on 47 river inundation areas estimated from 47 Landsat TM images. The root mean square errors (RMSE) in the estimated water surface elevations were about 5 cm and 4 cm at the KM and CC sites, respectively. The estimated 47 pairs of water surface elevations were substituted into an objective function formed by the Bernoulli

equation of gradually varied open channel flow. The nonlinear global optimization function embedded in Mathematica (i.e., NMinimize) was applied to solve the Manning's coefficient through minimizing the objective function value. Finally the river SDR curve was constructed at the KM site using the solved Manning's coefficient and Manning's equation, and employed to estimate river discharges. The root mean square error (RMSE) in the estimated river discharges against the USGS measured river discharges is $112.4 \text{ m}^3/\text{s}$. To consider the variation of the Manning's coefficient in the vertical direction, this study also suggested a power-law function to describe the vertical decline of the Manning's coefficient with the water level from the channel bed lowest elevation to the bank-full level. The constructed SDR curve with the vertical variation of the Manning's coefficient reduced the RMSE in the estimated river discharges to $83.9 \text{ m}^3/\text{s}$.

In summary, the proposed method to construct the SDR curve using the solved Manning's coefficient from the energy-balance-equation-based objective function is effective and feasible. Actually using the energy conservation equation (i.e., the Bernoulli equation) to solve downstream flow depth and discharge is one commonly used approach in the open channel flow, e.g., HEC-2 and HEC-RAS (Sturm, 2001). The difference is that to use the energy conservation equation, we should first have channel geometry information and the Manning's coefficient. The approach presented in this study could be considered as an inverse problem for solving the Manning's coefficient from estimated water surface elevations based on the energy conservation equation. One advantage of the approach is that no ground measurement of either river stage or river discharge is needed. One single Landsat image can provide inundation area estimations along a river at two cross sections simultaneously, and thus water surface elevations at upstream and downstream cross sections at the same time can be retrieved from the Landsat measured inundation areas based on the constructed IARSR curves. The simultaneous water surface elevations at upstream and downstream cross sections are critical for applying the energy conservation equation. The methodology developed in this study is applicable to both optical and microwave satellite images. If river stage or water surface elevation can be measured directly from satellites (e.g., altimeter and lidar), the steps in the proposed method to estimate river stage or water surface elevation from satellite measured inundation area are no longer necessary. The other steps to construct the SDR curves are

still useful and valid. A future study will be carried out to employ altimetry data for constructing the SDR curves using the method developed in this study.

In this study, we only constructed the stage-discharge rating (SDR) curve for flow level less than the bank-full condition at the KM site. Because if water level is above the bank-full level, we need to modify the energy balance equation to include both flows in the main channel and the floodplain. Also the impact of the floodplain on the mean Manning's coefficient should also be considered. These issues are beyond the scope of this paper and deserve a future study. Nonetheless, the methodology presented in this study is still valid and useful for constructing the SDR curves as water level is above the bank-full condition.

Acknowledgement

This research was partially funded by the University of North Texas (UNT) Research Opportunity Program (ROP) Grant (F. Pan) and Open Fund from State Key Laboratory of Remote Sensing Science, Chinese Academy of Sciences (Grant No. OFSLRSS201403, F. Pan). Useful comments were provided by editor K. Georgakakos, associate editor G. Duan, and two anonymous referees.

References

- Alessandrini, V., Bernardi, G., Todini, E., 2013. An operational approach to real-time dynamic measurement of discharge. *Hydrolog. Res.* 44, 953–964.
- Al-Khudairy, D.H.A., Leemhuis, C., Hoffmann, V., Shepherd, I.M., Calaon, R., Thompson, J.R., Gavin, H., Casca-Tucker, D.L., Zalidis, G., Bilas, G., Papadimos, D., 2002. Monitoring wetland ditch water levels using landsat TM and ground-based measurements. *Photogramm. Eng. Remote Sens.* 68, 809–818.
- Alsdorf, D.E., Rodriguez, E., Lettenmaier, D., 2007. Measuring surface water from space. *Rev. Geophys.* 45, RG2002. <http://dx.doi.org/10.1029/2006RG000197>.
- Andreadis, K.M., Clark, E.A., Lettenmaier, D.P., Alsdorf, D.E., 2007. Prospects for river discharge and depth estimation through assimilation of swath-altimetry into a raster-based hydrodynamics model. *Geophys. Res. Lett.* 34. <http://dx.doi.org/10.1029/2007GL029721>.
- Ashmore, P., Sauks, E., 2006. Prediction of discharge from water surface width in a braided river with implications for at-a-station hydraulic geometry. *Water Resour. Res.* 42 (W03406). <http://dx.doi.org/10.1029/2005WR003993>.
- Bates, P.D., Horritt, M.S., Smith, C.N., Mason, D.C., 1997. Integrating remote sensing observations of flood hydrology and hydraulic modeling. *Hydrolog. Process.* 11, 1777–1795.
- Bates, P.D., Wilson, M.D., Horritt, M.S., Mason, D.C., Holden, N., Currie, A., 2006. Reach scale floodplain inundation dynamics observed using airborne synthetic aperture radar imagery: data analysis and modeling. *J. Hydrol.* 328, 306–318.
- Becker, J.J., Sandwell, D.T., Smith, W.H.F., Braud, J., Binder, B., Depner, J., Fabre, D., Factor, J., Ingalls, S., Kim, S.H., Ladner, R., Marks, K., Nelson, S., Pharaoh, A., Trimmer, R., Von Rosenberg, J., Wallace, G., Weatherall, P., 2009. Global bathymetry and elevation data at 30 arc second resolution: SRTM30_PLUS. *Maine Geodesy* 32, 355–371.
- Bhang, K.J., Schwartz, F.W., Park, S.-S., 2010. Estimating historic lake stages from one-time snapshot, the shuttle radar topography mission of 2000. *Hydrolog. Process.* 24, 1834–1843.
- Bhowmik, N.G., Schicht, R.J., 1979. Bank erosion of the Illinois River. Illinois State Water Survey Report Investigat. 92.
- Bhowmik, N.G., Soong, D., 2000. Bank erosion survey of the Illinois River. Illinois State Water Survey, CR, 2000–2011.
- Birkett, C.M., Mertes, L.A.K., Dunne, T., Costa, M.H., Jasinski, M.J., 2002. Surface water dynamics in the Amazon Basin: application of satellite radar altimetry. *J. Geophys. Res. –Atmospheres* 107 (D20) 8059.
- Biancamaria, S., Lettenmaier, D.P., Pavelsky, T.M., 2015. The SWOT mission and its capabilities for land hydrology. *Surv. Geophys.* 1–31. <http://dx.doi.org/10.1007/s10712-015-9346-y>.
- Bjerkle, D.M., Dingman, S.L., Vorosmarty, C.J., Holster, C.H., Congalton, R.G., 2003. Evaluating the potential for measuring river discharge from space. *J. Hydrol.* 278, 17–38.
- Bjerkle, D.M., Moller, D., Smith, L.C., Dingman, S.L., 2005. Estimating discharge in rivers using remotely sensed hydraulic information. *J. Hydrol.* 309, 191–209.
- Braca, G., 2008. Stage-Discharge Relationships in Open Channels: Practices and Problems. FORALPS Technical Report, 11. Universita degli Studi di Trento, Dipartimento di Ingegneria Civile e Ambientale, Trento, Italy.
- Brakenridge, G.R., Tracy, B.T., Knox, J.C., 1998. Orbital SAR remote sensing of a river flood wave. *Int. J. Remote Sens.* 19, 1439–1445.
- Brakenridge, G.R., Nghiem, S.V., Anderson, E., Chien, S., 2005. Spacebased measurement of river runoff. *Eos, Trans., Am. Geophys. Union* 86 (185), 188.
- Brakenridge, G.R., Nghiem, S.V., Anderson, E., Mic, R., 2007. Orbital microwave measurement of river discharge and ice status. *Water Resour. Res.* 43 (W04405). <http://dx.doi.org/10.1029/2006WR005238>.
- Brivio, P.A., Colombo, R., Maggi, M., Tomasoni, R., 2002. Integration of remote sensing data and GIS for accurate mapping of flooded areas. *Int. J. Remote Sens.* 23, 429–441.
- Buchanan, T.J., Somers, W.P., 1969. Discharge Measurements at Gaging Stations. Techniques of Water-Resources Investigation of the United States Geological Survey, TWRI 3, A8.
- Calmant, S., Seyler, F., 2006. Continental surface waters from satellite altimetry. *C.R. Geosci.* 338, 1113–1122.
- Cai, X., Gan, W., Ji, W., Zhao, X., Wang, X., Chen, X., 2015. Optimizing remote sensing-based level-area modeling of large lake wetlands: case study of Poyang Lake. *IEEE J. Selected Top. Appl. Earth Observ. Remote Sens.* 8, 471–479.
- Chiu, C.L., Abidin Said, C.A., 1995. Maximum and mean velocities and entropy in open-channel flow. *J. Hydraul. Eng.* 121 (1), 26–35.
- Cloke, H.L., Pappenberger, F., 2009. Ensemble flood forecasting: a review. *J. Hydrol.* 375 (3–4), 613–626.
- Coe, M.T., Birkett, C.M., 2004. Calculation of river discharge and prediction of lake height from satellite radar altimetry: example for the Lake Chad basin. *Water Resour. Res.* 40 (W10205). <http://dx.doi.org/10.1029/2003WR002543>.
- Costa, J.E., Spicer, K.R., Cheng, R.T., Haeni, F.P., Melcher, N.B., Thurman, E.M., Plant, W.J., Keller, W.C., 2000. Measuring stream discharge by non-contact methods: a proof-of-concept experiment. *Geophys. Res. Lett.* 27 (4), 553–556.
- Domeneghetti, A., Tarpanelli, A., Brocca, L., Barbetta, S., Moramarco, T., Castellarin, A., Brath, A., 2014. The use of remote sensing-derived water surface data for hydraulic model calibration. *Remote Sens. Environ.* 149, 130–141.
- Durand, M., Andreadis, K.M., Alsdorf, D.E., Lettenmaier, D.P., Moller, D., Wilson, M., 2008. Estimation of bathymetric depth and slope from data assimilation of swath altimetry into a hydrodynamic model. *Geophys. Res. Lett.* 35 (L20401). <http://dx.doi.org/10.1029/2008GL034150>.
- Durand, M., Neal, J., Rodriguez, E., Andreadis, K.M., Smith, L.C., Yoon, Y., 2014. Estimating reach-averaged discharge for the River Severn from measurements of river water surface elevation and slope. *J. Hydrol.* 511, 92–104.
- Farina, G., Alvisi, S., Franchini, M., Moramarco, T., 2014. Three methods for estimating the entropy parameter M based on a decreasing number of velocity measurements in a river cross section. *Entropy Hydrolog.* 16 (5), 2512–2529.
- Fekete, B.M., Vörösmarty, C.J., 2007. The current status of global river discharge monitoring and potential new technologies complementing traditional discharge measurements. In: Predictions in Ungauged Basins: PUB Kick-off (Proceedings of the PUB Kick-off meeting held in Brasilia, 20–22 November 2002. IAHS Publication, p. 309.
- Frazier, P.S., Page, K.J., 2000. Water body detection and delineation with Landsat TM data. *Photogramm. Eng. Remote Sens.* 66 (12), 1461–1467.
- Garambois, P.A., Monnier, J., 2015. Inference of effective river properties from remotely sensed observations of water surface. *Adv. Water Resour.* 79, 103–120.
- Gesch, D.B., 2007. The national elevation dataset. In: Maune, D. (Ed.), Digital Elevation Model Technologies and Applications: The DEM Users Manual, second ed. American Society for Photogrammetry and Remote Sensing, Bethesda, Maryland, pp. 99–118.
- Gesch, D., Oimoen, M., Greenlee, S., Nelson, C., Steuck, M., Tyler, D., 2002. The national elevation dataset. *Photogramm. Eng. Remote Sens.* 68 (1), 5–11.
- Gleason, C.J., Smith, L.C., 2014. Toward global mapping of river discharge using satellite images and at-many-stations hydraulic geometry. *Proc. Natl. Acad. Sci.* 111 (13), 4788–4791.
- Gleason, C.J., Smith, L.C., Lee, J., 2014. Retrieval of river discharge solely from satellite imagery and at-many-stations hydraulic geometry: sensitivity to river form and optimization parameters. *Water Resour. Res.* 50 (12), 9604–9619.
- Gleason, C.J., Wang, J., 2015. Theoretical basis for at-many-stations hydraulic geometry. *Geophys. Res. Lett.* 42 (17), 7107–7114.
- Hamilton, S.K., Sipple, S.J., Melack, J.M., 1996. Inundation patterns in the Pantanal wetland of South America determined from passive microwave remote sensing. *Arch. Hydrobiol.* 137, 115–141.
- Hannah, D.M., Demuth, S., van Lanen, H.A.J., Looser, U., Prudhomme, C., Rees, G., Stahl, K., Tallaksen, L.M., 2011. Large-scale river flow archives: importance, current status and future needs. *Hydrolog. Process.* 25, 1191–1200.
- Henderson, F.M., 1966. Open Channel Flow. The Macmillan Co., New York.
- Herschy, R.W., 1995. Streamflow Measurement, second ed. Chapman & Hall.
- Hirsch, R.M., Costa, J.E., 2004. U.S. stream flow measurement and data dissemination improve. *EOS, Trans., Am. Geophys. Union* 85 (20), 197–203.
- Hornberger, G.M., Wiberg, P.L., Raffensperger, J.P., D'Odorico, P., 2014. Elements of Physical Hydrology. Johns Hopkins University Press, Baltimore, Maryland.
- Horritt, M.S., Bates, P.D., 2002. Evaluation of 1D and 2D numerical models for predicting river flood inundation. *J. Hydrol.* 268 (1–4), 87–99.
- IAHS Ad Hoc Committee, 2001. Global water data: a newly endangered species, *EOS Transactions. Am. Geophys. Union* 82 (5), 54, 56, 58.
- Jarihani, A.A., Callow, J.N., Johansen, K., Gouweleeuw, B., 2013. Evaluation of multiple satellite altimetry data for studying inland water bodies and river floods. *J. Hydrol.* 505, 78–90.
- Jakobsson, M., Macnab, R., Mayer, L., Anderson, R., Edwards, M., Hatzky, J., Schenke, H.W., Johnson, P., 2008. An improved bathymetric portrayal of the Arctic Ocean: implications for ocean modeling and geological, geophysical and oceanographic analyses. *Geophys. Res. Lett.* 35. <http://dx.doi.org/10.1029/2008GL033520>.

- Jung, Y., Merwade, V., Yeo, K., Shin, Y., Lee, S., 2013. An approach using a 1D hydraulic model, Landsat imaging and generalized likelihood uncertainty estimation for an approximation of flood discharge. *Water* 5, 1598–1621.
- Keys, R.G., 1981. Cubic convolution interpolation for digital image processing. *IEEE Trans. Acoust. Speech Signal Process.* 29 (6), 1153–1160.
- Kennedy, E.J., 1984. Discharge Ratings at Gaging Stations: U.S. Geological Survey Techniques of Water-Resources Investigation Report, Book 3, Ch. A10, 59p.
- Koblinsky, C.J., Clarke, R.T., Brenner, A.C., Frey, H., 1993. Measurement of river level variations with satellite altimetry. *Water Resour. Res.* 29 (6), 1839–1848.
- Kouraev, A.V., Zakharova, E.A., Samain, O., Mognard, N.M., Cazenave, C., 2004. Ob’ river discharge from TOPEX/Poseidon satellite altimetry (1992–2002). *Remote Sens. Environ.* 93, 238–245.
- Leon, J.G., Calmant, S., Seyler, F., Bonnet, M.P., Cauhopé, M., Frappart, F., Filizola, N., Fraize, P., 2006. Rating curves and estimation of average water depth at the upper Negro River based on satellite altimeter data and modeled discharges. *J. Hydrol.* 328, 481–496.
- Matgen, P., Henry, J.P., Pappenberger, F., De Fraipont, P., Hoffmann, L., Pfister, L., 2004. Uncertainty in calibrating flood propagation models with flood boundaries observed from synthetic aperture radar imagery. In: Proceedings of the 20th Congress of the International Society of Photogrammetry and Remote Sensing, Istanbul, Turkey, pp. 352–358.
- Matgen, P., Schumann, G., Henry, J.B., Hoffmann, L., Pfister, L., 2007. Integration of SAR-derived river inundation areas, high-precision topographic data and a river flow model toward near real-time flood management. *Int. J. Appl. Earth Obs. Geoinf.* 9 (3), 247–263.
- Moramarco, T., Singh, V., 2010. Formulation of the entropy parameter based on hydraulic and geometric characteristics of river cross sections. *J. Hydrol. Eng.* 15 (10), 852–858.
- Morlock, S.E. (1996). Evaluation of Acoustic Doppler Current Profiler Measurements of River Discharge, Water-Resour. Investig. Rep. 95-4218, U.S. Geol. Survey, Washington, DC, 37pp.
- Mosley, M.P., McKerchar, A.I., 1992. Streamflow. In: Maidment, D.R. (Ed.), *Handbook of Hydrology*. McGraw-Hill, New York.
- Mueller, D.S., 2003. Field evaluation of boat-mounted acoustic doppler instruments used to measure stream flow. In: Proc. IEEE Seventh Working Conference on Current Measurement Technology, March 2003, San Diego, Calif, pp. 30–34.
- Mueller, D.S., Wagner, C.R., 2006. Application of the Loop Method for Correcting Acoustic Doppler Current Profiler Discharge Measurements Biased by Sediment Transport: U.S. Geological Survey Scientific Investigations Report 2006-5079, 26p.
- Mueller, D.S., Wagner, C.R., Rehmel, M.S., Oberg K.A., Rainville, F., 2013. Measuring Discharge with Acoustic Doppler Current Profilers from a Moving Boat: Techniques and Methods 3-A22, U.S. Geol. Survey, Washington, DC.
- Nelder, J.A., Mead, R., 1965. A simplex method for function minimization. *Comput. J.* 7, 308–313.
- Oberg, K.A., Mueller, D.S., 2007. Validation of stream-flow measurements made with acoustic Doppler current profilers. *J. Hydraul. Eng.* 133 (12), 1421–1432.
- Olson, S.A., Norris, J.M., 2005. U.S. Geological Survey Streamgaging, U.S. Geological Survey Fact Sheet 2005-3131.
- Overton, I.C., 2005. Modeling floodplain inundation on a regulated river: integrating GIS, remote sensing and hydrological models. *River Res. Appl.* 21, 91–1001.
- Pan, F., Nichols, J., 2013. Remote sensing of river stage using the cross sectional inundation area – river stage relationship (IARSR) constructed from digital elevation model data. *Hydrol. Process.* 27, 3596–3606.
- Pan, F., 2013. Remote sensing of river stage and discharge. SPIE Newsroom. <http://dx.doi.org/10.1117/2.1201212.04611>.
- Pan, F., Liao, J., Li, X., Guo, H., 2013. Application of the inundation area-lake level rating curves constructed from the SRTM DEM to retrieving lake levels from satellite measured inundation areas. *Comput. Geosci.* 52 (168–176), 2013.
- Pavelsky, T.M., 2014. Using width-based rating curves from spatially discontinuous satellite imagery to monitor river discharge. *Hydrol. Process.* 28 (6), 3035–3040.
- Pavelsky, T.M., Durand, M.T., Andreidis, K.M., Beighley, R.E., Paiva, R.D., Allen, G.H., Miller, Z.F., 2014. Assessing the potential global extent of SWOT river discharge observations. *J. Hydrol.* 519, 1516–1525.
- Pietroniro, A., Prowse, T., Peters, D.L., 1999. Hydrologic assessment of an inland freshwater delta using multi-temporal satellite remote sensing. *Hydrol. Process.* 13, 2483–2498.
- Rantz, S.E., others., 1982a. Measurement and Computation of Streamflow, Volume 1 Measurement of Stage and Discharge. U.S. Geological Survey Water Supply Paper 2175.
- Rantz, S.E., others., 1982b. Measurement and Computation of Streamflow, Volume 2 Computation of Discharge. U.S. Geological Survey Water Supply Paper 2175.
- Rogala, J.T., 1999. Methodologies Employed for Bathymetric Mapping and Sediment Characterization as Part of the Upper Mississippi River System Navigation Feasibility Study, ENV Report 13, Interim Report for the Upper Mississippi River – Illinois Waterway System Navigation Study; prepared for U.S. Army Engineers District, Rock Island, U.S. Army Engineers District, St. Louis, and U.S. Army Engineers District, St. Paul.
- Roux, H., Dartus, D., Source, D., 2008. Sensitivity analysis and predictive uncertainty using inundation observations for parameter estimation in open-channel inverse problem. *J. Hydraul. Eng.* 134 (5), 541–549.
- Sauer, V.B., 2002. Standards for the Analysis and Processing of Surface-Water Data and Information using Electronic Methods. U.S. Geological Survey Water-Resources Investigations Report 01-4044, 91p.
- Schumann, G., Pappenberger, F., Matgen, P., 2008a. Estimating uncertainty associated with water stages from a single SAR image. *Adv. Water Resour.* 31 (8), 1038–1047.
- Schumann, G., Pappenberger, F., Matgen, P., 2008b. Conditioning water stages from satellite imagery on uncertain data points. *IEEE Geosci. Remote Sens. Lett.* 5 (4), 810–813.
- Schumann, G., Bates, P.D., Horritt, M.S., Matgen, P., Pappenberger, F., 2009. Progress in integration of remote sensing-derived flood extent and stage data and hydraulic models. *Rev. Geophys.* 47, RG4001.
- Simpson, M., 2001. Discharge Measurements using a Broad-Bank Acoustic Doppler Current Profiler, Open-File Rep. 01-01, U.S. Geol. Survey, Washington, DC, 123pp.
- Simpson, M.R., Oltmann, R.N., 1993. Discharge Measurement using an Acoustic Doppler Current Profiler: U.S. Geological Survey Water-Supply Paper 2395, 34p.
- Smith, L.C., 1997. Satellite remote sensing of river inundation area, stage, and discharge: a review. *Hydrolog. Process.* 11, 1427–1439.
- Smith, L.C., Isacks, B.L., Forster, R.R., Bloom, A.L., Preuss, I., 1995. Estimation of discharge from braided glacial rivers using ERS-1 synthetic aperture radar: first results. *Water Resour. Res.* 31, 1325–1329.
- Smith, L.C., Isacks, B.L., Bloom, A.L., Murray, A.B., 1996. Estimation of discharge from three braided rivers using synthetic aperture radar (SAR) satellite imagery: potential applications to ungauged basins. *Water Resour. Res.* 32, 2021–2034.
- Smith, L.C., Pavelsky, T.M., 2008. Estimation of river discharge, propagation speed, and hydraulic geometry from space: Lena River, Siberia. *Water Resour. Res.* 44 (W03427). <http://dx.doi.org/10.1029/2007WR006133>.
- Smith, L.C., Pavelsky, T.M., 2009. Remote sensing of volumetric storage changes in lakes. *Earth Surf. Proc. Land.* 34, 1353–1358.
- Smith, W.H.F., Sandwell, D.T., 1997. Global sea floor topography from satellite altimetry and ship depth soundings. *Science* 227, 1956–1962.
- Sturm, T.W., 2001. Open Channel Hydraulics. McGraw-Hill, New York.
- Tarpanelli, A., Barbetta, S., Brocca, L., Moramarco, T., 2013. River discharge estimation by using altimetry data and simplified flood routing modeling. *Remote Sens.* 5 (9), 4145–4162.
- Temimi, M., Leconte, R., Brissette, F., Chaouch, N., 2005. Flood monitoring over the Mackenzie River Basin using passive microwave data. *Remote Sens. Environ.* 98, 344–355.
- Vorosmarty, C.J., Willmott, C.J., Choudhury, B.J., Schloss, A.L., Stearns, T.K., Robeson, S.M., Dorman, T.J., 1996. Analyzing the discharge regime of a large tropical river through remote sensing, ground-based climatic data and modeling. *Water Resour. Res.* 32, 3137–3150.
- Xu, K.Q., Zhang, J.Q., Watanabe, M., Sun, C.P., 2004. Estimating river discharge from very high-resolution satellite data: a case study in the Yangtze River, China. *Hydrolog. Process.* 18, 1927–1939.
- Zhang, J.Q., Xu, K.Q., Watanabe, M., Yang, Y.H., Chen, X.W., 2004. Estimation of river discharge from non-trapezoidal open channel using QuickBird-2 satellite imagery. *Hydrol. Sci. J.* 49, 247–260.